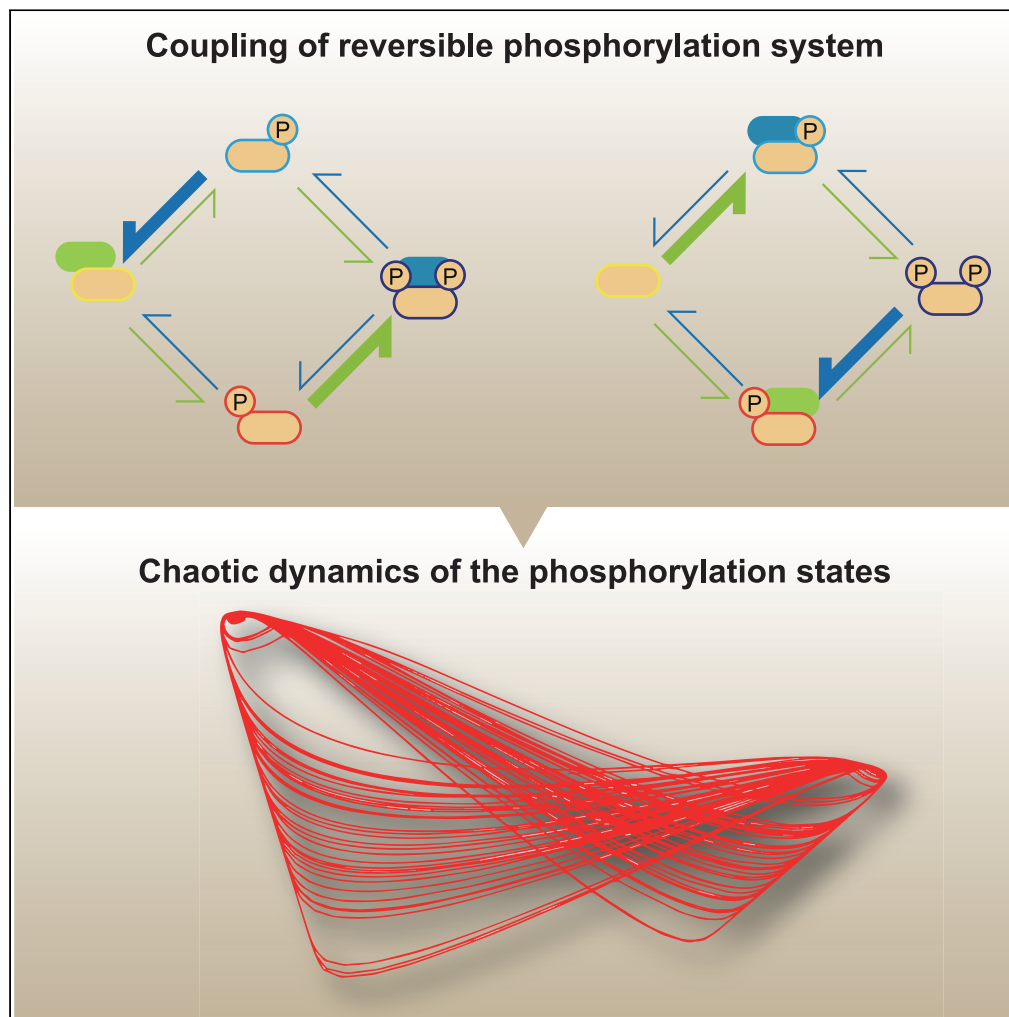


Article

A design principle for posttranslational chaotic oscillators



Hiroto Q.
Yamaguchi, Koji L.
Ode, Hiroki R.
Ueda

uedah-ky@umin.ac.jp

Highlights

Two substrates with reversible two-site phosphorylation can exhibit chaos behavior

The chaos does not require autocatalysis or allosteric regulation of enzymes

The chaos is a result of the coupling of two substrates via enzyme availability

Yamaguchi et al., iScience 24,
101946
January 22, 2021 © 2020 The
Authors.
[https://doi.org/10.1016/
j.isci.2020.101946](https://doi.org/10.1016/j.isci.2020.101946)

Article

A design principle for posttranslational chaotic oscillators

Hiroto Q. Yamaguchi,^{1,2,3} Koji L. Ode,^{1,4} and Hiroki R. Ueda^{1,4,5,*}

Summary

Chaos behavior has been observed in various cellular and molecular processes. Here, we modeled reversible phosphorylation dynamics to elucidate a design principle for autonomous chaos generation that may arise from generic enzymatic reactions. A comprehensive parameter search demonstrated that the reaction system composed of a set of kinases and phosphatases and two substrates with two modification sites exhibits chaos behavior. All reactions are described according to the Michaelis-Menten reaction scheme without exotic functions being applied to enzymes and substrates. Clustering analysis of parameter sets that can generate chaos behavior revealed the existence of motif structures. These chaos motifs allow the two-substrate species to interact via enzyme availability and constrain the two substrates' dynamic changes in phosphorylation status so that they occur at different timescales. This chaos motif structure is found in several enzymatic reactions, suggesting that chaos behavior may underlie cellular autonomy in a variety of biochemical systems.

Introduction

The spontaneous activation of chemical reactions is the basis of cellular autonomy. Biological oscillators play an important role in the control of the autonomous and temporal activities that occur in cells. Examples include autonomous rhythmicity observed in the circadian cellular clock process (Nagoshi et al., 2004), cell cycle progression (Murray and Kirschner, 1989), and rhythmic neuronal firing (Izhikevich, 2007). Such activities can span timescales from milliseconds to hours. Biological oscillators are also thought to play an important role in autonomous pattern formation from body segmentation in mammals (cm scale) (Palmeirim et al., 1997) and the positioning of cell division machinery inside unicellular prokaryotes (μm scale) (Raskin and de Boer, 1999). These oscillators are often modeled as feedback loops composed of genetic, biochemical, and cellular events that exhibit limit cycle oscillation over a wide period range (Goldbeter, 2002). Biological systems are composed of multiple oscillators, which in many cases interact with each other. For example, it was recently demonstrated that the segmentation clock period is modulated by intercellular coupling of genetic oscillators (Yoshioka-Kobayashi et al., 2020). Such coupling also occurs within cells among oscillators that drive various physiological functions, e.g., circadian clocks influence cell cycle progression (Matsuo et al., 2003; Yang et al., 2010) and, in turn, cell cycle phase influences the circadian clock (Bieler et al., 2014). Such coupling of multiple oscillators may help produce robust oscillation (Droin et al., 2019; Yan and Goldbeter, 2019b).

In certain conditions, coupled oscillators may exhibit more complex dynamics including multirhythmicity and chaos behavior (Gerard and Goldbeter, 2012; Yan and Goldbeter, 2019a). Indeed, chaos behavior may play a fundamental role in the functioning of biological systems; it has been suggested that autonomous and complex systems (such as living systems) converge on the edge of chaos (Kauffman, 1992; Langton, 1990). Autonomous chaos behavior has been observed and modeled extensively in various biological layers; early examples include the peroxidase enzymatic reaction (Olsen and Degn, 1977), neuronal firing (Aihara et al., 1985; Skarda and Freeman, 1987), and cAMP signaling in *Dictyostelium* (Durstion, 1974; Martiel and Goldbeter, 1985). Chaos behavior continues to be recognized for its importance in modern biology. For example, a recent modeling study of the sleep-wake cycle suggested that the transition between chaos behavior and regular oscillation may underlie the state alteration from sleep-associated to wake-associated neuronal firing patterns (Rasmussen et al., 2017). In such studies, mathematical models are used to understand and predict how complex and autonomous behavior occurs when cellular and molecular activities are modulated. However, it is often difficult to understand how chaos behavior arises from

¹Department of Systems Pharmacology, Graduate School of Medicine, the University of Tokyo, Hongo 7-3-1, Bunkyo-ku, Tokyo, 113-0033, Japan

²Center for Information and Neural Networks, National Institute of Information and Communications Technology, 1-4 Yamadaoka, Suita, Osaka 565-0871, Japan

³Graduate School of Frontier Biosciences, Osaka University, 1-3 Yamadaoka, Suita, Osaka 565-0871, Japan

⁴Laboratory for Synthetic Biology, RIKEN Center for Biosystems Dynamics Research, 1-3 Yamadaoka, Suita, Osaka 565-0871, Japan

⁵Lead Contact

*Correspondence:

uedah-ky@umin.ac.jp

<https://doi.org/10.1016/j.isci.2020.101946>



a biochemical reaction system because the biological networks that give rise to chaos behavior can involve multiple gene expression networks, cell-cell interactions, and the complex regulation of molecules.

In modern research, a synthetic biology approach is increasingly being employed to gain mechanistic insights into the autonomous generation of complex behaviors from biological components. In this approach, the aim is to design complex responses from relatively simple model systems. Protein networks shaped by enzymatic reactions and protein-protein interactions have recently been studied using a synthetic biology approach, leading to the *de novo* design of protein logical circuits (Chen et al., 2020; Fink et al., 2019; Gao et al., 2018). Complex responses have also been observed in nuclear-free cytosolic extract systems, where protein networks, rather than genetic circuits, play a role to elicit autonomous responses (Pomerening et al., 2003, 2005). Therefore, the design of protein networks in cells may improve understanding of how the complex responses exhibited by individual cells originated. Mathematical models can facilitate the design of synthetic protein-based circuits for autonomous activity including chaos. These models must be detailed enough to map to measurable biochemical parameters but also contain a small enough number of components to facilitate experimental design.

In the present study, we use modeling of biological autonomous chaos to interrogate the general design principles of biological chaos that can be realized in a set of ubiquitous molecular systems. Reversible phosphorylation is a well-understood mechanism by which protein activity is regulated. A typical model of reversible phosphorylation assumes a set of antagonizing enzymes (a kinase and a phosphatase) and a substrate (Conradi and Shiu, 2018; Kholodenko, 2006). The enzymes catalyze the phosphorylation and dephosphorylation of the substrate following the Michaelis-Menten reaction scheme. Despite its simplicity and generality, this reaction scheme can generate various complex behaviors; in particular, reversible phosphorylation with two or more modification sites in one-substrate molecule can exhibit biostability (Markevich et al., 2004), multistability (Thomson and Gunawardena, 2009), and autonomous oscillation (Conradi et al., 2019; Jolley et al., 2012; Suwanmajo and Krishnan, 2015). In addition, the spatiotemporal dynamics of this system include traveling waves (Markevich et al., 2006) and the Turing pattern (Sugai et al., 2017). The generic applicability of the reversible phosphorylation model to the modeling of various types of posttranslational modification enables researchers to investigate a typical molecular mechanism that produces complex behaviors from a combination of simple enzymatic reactions.

Specifically, we demonstrate here that chaos behavior can arise from a reversible phosphorylation model entirely described by the Michaelis-Menten reaction scheme. The system does not assume typical allosteric regulation of enzymes in which the enzymes' reaction rates are actively modulated by the substrate, explicit autocatalytic activities, or any other exotic control of the enzymes. The complexity of our model system arises from its composition, which includes two-substrate species each of which has two modification sites. We found that typical combinations of reaction parameters create chaos motifs that allow each of the two substrates to behave as an oscillator and to couple with each other through the availability of shared enzymes. This motif structure can be found in several well-known kinases. Therefore, our model will help researchers to identify and perhaps design possible enzymatic reaction components that can induce autonomous complex outputs in cells.

Results

A coupled dual-phosphorylation system shows chaos behavior

The simplest type of reversible phosphorylation scheme is a system with a single substrate that has one phosphorylation site (Figure S1A). However, this scheme can be modeled as a one-dimensional system by applying the Michaelis-Menten approximation, and thus, oscillation and chaos are impossible (Jolley et al., 2012; Strogatz, 1994). Therefore, we next consider a similar reversible phosphorylation system but single substrate contains two phosphorylation sites. In this system, we previously found that reversible two-site phosphorylation in a single substrate system can have a limit cycle oscillation (Jolley et al., 2012). We assessed whether the same system could exhibit chaos behavior. The system consists of a single substrate with two phosphorylation sites, which are phosphorylated and dephosphorylated by a kinase and a phosphatase, respectively (Figure S1A). All the reactions follow the Michaelis-Menten reaction scheme. Parameters were randomly sampled from an exponential distribution bounded between 1 and 1000 min⁻¹ for reaction rate constants (*k*) and between 0.01 and 1000 μM for binding constants (*K_m*). Note that a low *K_m* value indicates strong binding between an enzyme and the substrate. The parameter range corresponds to reasonable values typically used in other simulation studies (Chickarmane et al., 2007; Jolley et al., 2012; Liu

et al., 2011; Markevich et al., 2004; Qiao et al., 2007; Shankaran et al., 2009; Sugai et al., 2017) and within the distribution of k_{cat} and K_m values observed in various enzymes (Bar-Even et al., 2011). Through the numerical integration of the system with 10,000,000,000 randomly sampled parameter sets, we identified 12,636,210 parameter sets that exhibit limit cycle oscillation but did not find any parameters that exhibit chaos behavior, suggesting that the single-substrate system is not complex enough to include chaos behavior.

We therefore considered a dual-substrate system consisting of two types of substrate, named S_a and S_b (Figure 1A). Each substrate has two phosphorylation sites that are modified reversibly by a shared kinase (E) and a shared phosphatase (F). S_a has four phosphorylation states, named S_{a00} , S_{a01} , S_{a10} , and S_{a11} ; S_b also has four phosphorylation states, named S_{b00} , S_{b01} , S_{b10} , and S_{b11} . The states S_{a00} and S_{b00} are unphosphorylated substrate states, whereas S_{a01} , S_{a10} , S_{b01} , and S_{b10} are substrate states with single phosphorylation at either one of the modification sites. The remaining states, S_{a11} and S_{b11} , are substrate states with phosphorylation at both of the two modification sites.

This dual-substrate system showed chaos behavior with some parameter sets (hereafter called “chaos parameter sets”). With chaos parameter sets, the system never converged to a stable state or limit cycle oscillation (Figure 1B). The chaos behavior was further validated by showing that small changes in the initial state could lead to a variety of different states after the system had evolved to a certain time (Figure 1C). The power spectrum of chaos orbitals showed a broad spectrum rather than a few peaks with strong power intensity (Figure 1D). These features distinguish the chaos parameter sets from parameters resulting in limit cycle oscillations (hereafter called “oscillation parameter sets”) (Figures S1B–S1D).

Conserved parameter motifs in the chaos parameter sets

To ascertain whether a specific parameter region was related to chaos behavior in the parameter space, chaos parameter sets were collected by a random parameter search within the same distribution of k_{cat} and K_m values described above. This random search revealed 4,818 chaos and 286,255 oscillation parameter sets from 13,269,134,692 randomly generated parameter sets ($\sim 0.0000363\%$ for chaos and $\sim 0.00216\%$ for oscillation parameter sets) (Figure 2A).

To identify a typical motif structure of the chaos parameter sets, hierarchical clustering analysis was performed on the collected chaos parameter sets. Seven clusters were defined by setting a threshold to the clustering dendrogram (Figure 2B). To elucidate the characteristic combination in each cluster, we identified the fast reaction rate based on the criterion that the probability of the corresponding k parameter exceeds a certain threshold (0.2; for details, see Transparent methods) at the highest parameter bin (1000 min^{-1}). Similarly, we identified the stable substrate-enzyme complex based on the criterion that the probability of corresponding K_m exceeds the threshold at the lowest parameter bin ($0.01 \mu\text{M}$). Figure 2C (upper section) shows a schematic view of the chaos parameter sets classified as cluster 1. This scheme highlights the positions of large k values (fast reaction speeds) and small K_m values (stable enzyme-substrate complex formation). The parameter distributions of clusters 2–7 are shown in Figure S2. The histograms in each panel indicate the parameter distributions (Figures 2C and S2).

We found that all the clusters included a shared motif structure in at least one part of the phosphorylation/dephosphorylation pathway (as highlighted by yellow coloring trimmed with green or orange in Figures 2C and S2 [discussed later]). The shared motif structure shown in Figure 2D is characterized by a fast reaction that produces stable binding of the substrate (S_{pos}) with either the kinase or phosphatase that is not the same enzyme catalyzed in the fast reaction (i.e., if the fast reaction is a phosphorylation reaction, the product is stably bound with a phosphatase not a kinase.) For example, in cluster 1 (Figure 2C), a kinase reaction with a high k_{a4} value produces S_{a11} , which involves stable binding with the phosphatase as indicated by the low K_{ma7} value. In the same way, the other motif is composed of a phosphatase reaction with a high k_{a5} value that produces S_{a00} , which involves stable binding with the kinase as indicated by a low K_{ma2} value.

Motif arrangements necessary for chaos behavior

The motifs can be categorized into two types (named motif A and B, respectively) by considering the symmetry of a state transition diagram (Figure 3A). In motif A, a fast reaction is assigned such that a fully phosphorylated (S_{00}) or fully dephosphorylated product (S_{11}) is produced. On the other hand, motif B is composed of a fast reaction that produces a single phosphorylated substrate (S_{01} or S_{10}). S_{00} and S_{11}

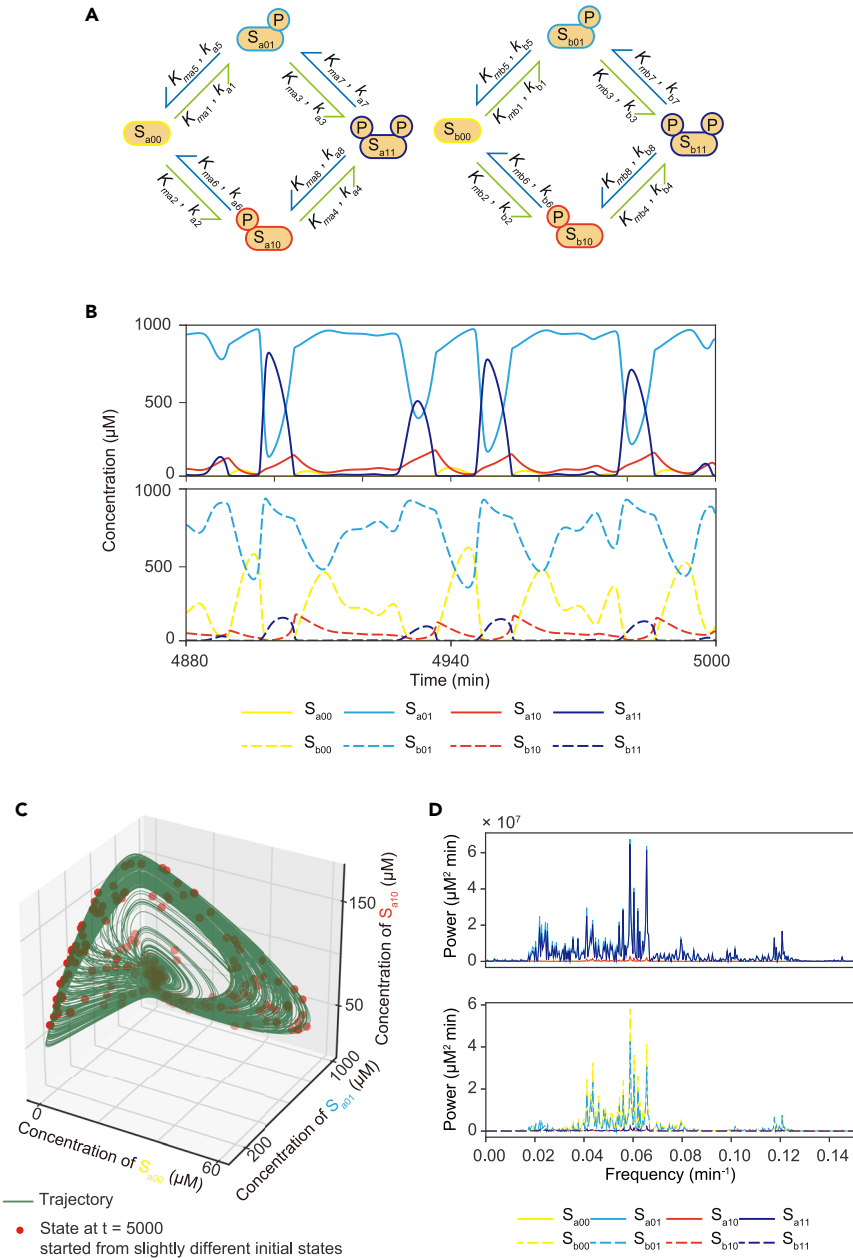


Figure 1. A coupled dual-phosphorylation system shows chaos behavior

(A) A reaction network comprising a two-substrate (i.e., S_a and S_b) system. Each substrate undergoes a reversible phosphorylation cycle at two residues. The phosphorylation (green arrows) and dephosphorylation (blue arrows) reactions are catalyzed by a shared kinase and phosphatase, respectively. All the reactions follow a Michaelis-Menten reaction scheme characterized by parameters for reaction speed k and enzyme-substrate affinity K_m .

(B) An example time course of chaotic phosphorylation dynamics.

(C) The example chaotic trajectory from $t = 0$ min to $t = 5,000$ min is projected to S_{a00} - S_{a01} - S_{a10} space (green line). Red dots indicate the phosphorylation states at $t = 5,000$ min obtained from 200 runs of the simulation with slightly different initial conditions.

(D) Power spectrum of the example chaotic trajectory analyzed by fast Fourier transform (FFT). See also [Figure S1](#).

can be converted by converting the kinase and phosphatase; thus, they have a symmetrical relationship. S_{01} and S_{10} are also symmetrical because they can be converted by converting the position of two phosphorylation residues. However, S_{00} cannot be converted into S_{01} or S_{10} by a symmetrical conversion because S_{00}

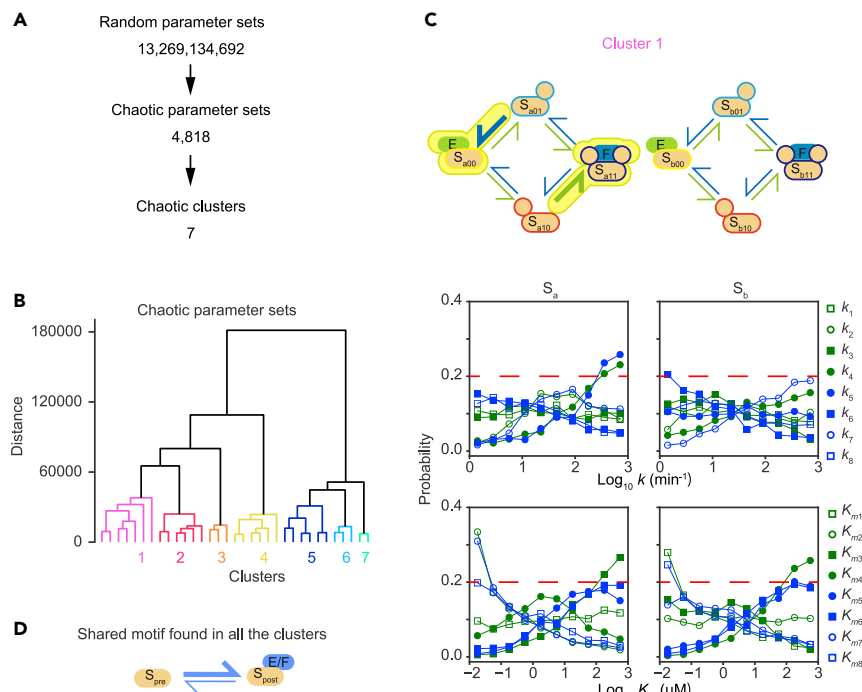


Figure 2. Shared motifs in chaotic parameter sets

(A) Workflow for chaotic motif identification.

(B) Clustering of chaotic parameter sets with Ward's algorithm. The chaotic parameter sets were standardized by considering phosphor-site symmetries.

(C) Schematic representation and parameter histograms for the largest cluster. Reaction constants (k) for which the distribution exceeds the probability 0.2 (red dotted lines) at the highest value are denoted as fast reactions. Michaelis constants (K_m) for which the distribution exceeds the probability 0.2 at the lowest value are denoted as high-affinity enzyme-substrate bindings. The fast reactions are shown as thick arrows, while the high-affinity bindings are indicated by attaching the kinase (E) or phosphatase (F) to the edge of the corresponding substrate species.

(D) A shared design motif found in all clusters. A fast reaction produces a substrate species that has high affinity with either E or F.

See also [Figure S2](#).

binds to and is a substrate for a kinase only. In contrast, S_{01} and S_{10} can bind to and be a substrate for either a kinase or a phosphatase. Similarly, S_{11} cannot be symmetrically converted to S_{01} or S_{10} . These asymmetries make motif A and motif B independent. Either type of motif can be found in each of the chaos clusters. In [Figures 1C](#) and [S2](#), motif A is highlighted in yellow trimmed with green and motif B is highlighted in yellow trimmed with orange.

To investigate whether the presence of a motif structure is important to chaos behavior in the two-substrate system, we performed a biased parameter search. Each motif could be placed into four symmetrical positions on a reaction diagram of each S_a and S_b substrate ([Figure 3A](#)). We tested a scenario in which each substrate could have up to two motif As and two motif Bs, respectively. According to the symmetry within the reaction diagram, 46 patterns of different motif biases cover all possible arrangements of motifs ([Figure 3B](#)). Among the 46 motif arrangements, 35 were more likely to show chaos behavior than a system without any motif bias. These 35 motif arrangements included those that correspond to the clustering analysis results (e.g., cluster 1–7). For example, a structure that has motif A in the positions $S_{a01} \rightarrow S_{a00}$ and $S_{a10} \rightarrow S_{a11}$ corresponds to cluster 1, 2, and 4 and shows a higher probability of having chaos behavior than in the parameter search without any motif bias ([Figure 3B](#): arrangement #4).

The biased parameter search suggested that motifs with specific arrangements contribute to chaos behavior ([Figure 3B](#)). First, the probability of chaos behavior increases when motif A or motif B are placed in rotationally symmetrical positions (e.g., conversion between $S_{00} \leftrightarrow S_{01}$ or between $S_{11} \leftrightarrow S_{10}$); arrangements #4, #6, and #7 show higher chaos probabilities as they contain two motif As in rotationally

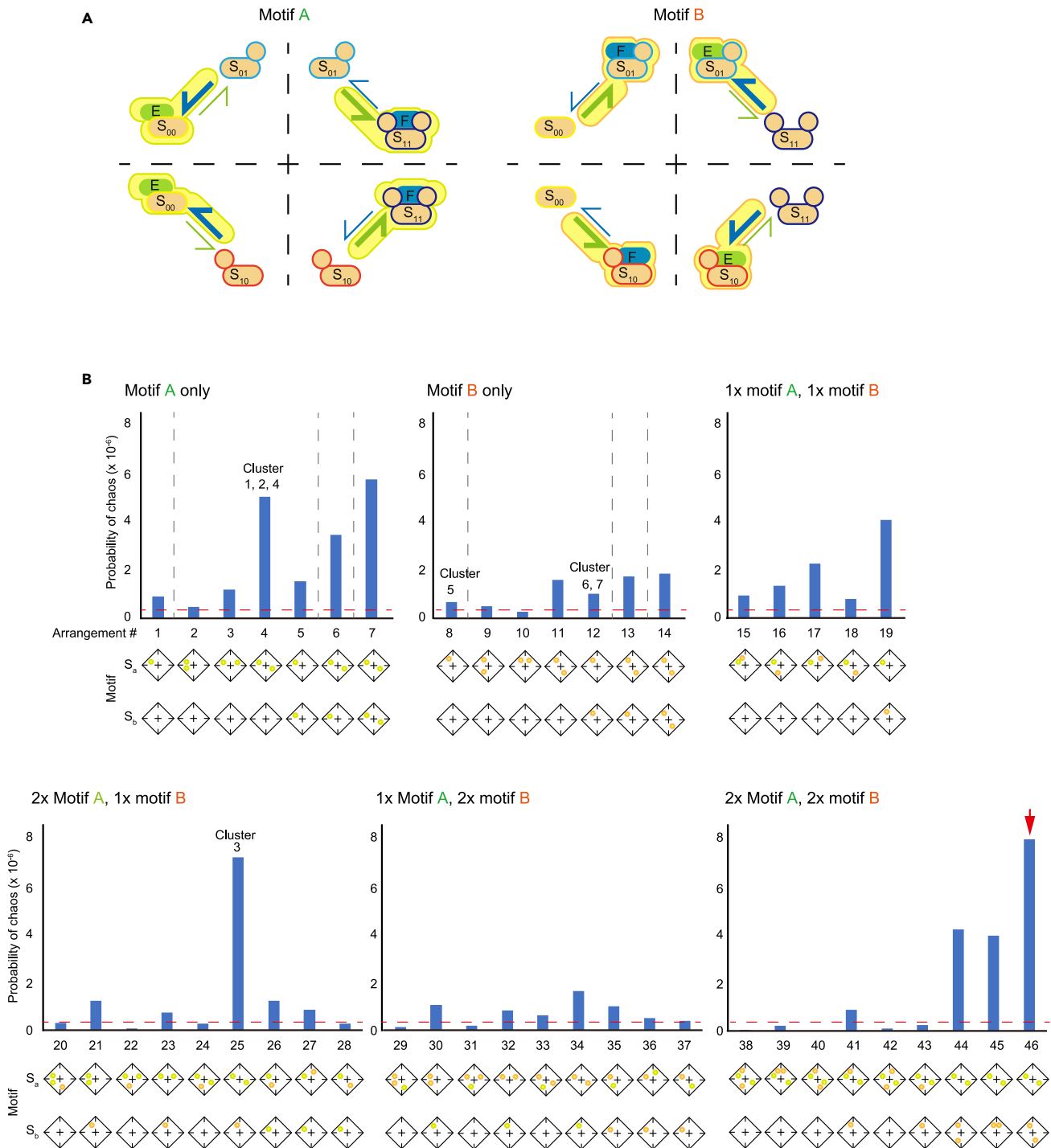


Figure 3. Functional significance of the number and arrangement of chaos motifs

(A) The chaos motif can be subdivided into two types. Motif A comprises either an unphosphorylated substrate (S_{00}) or fully phosphorylated substrate (S_{11}) as a high-affinity substrate that tightly binds to kinase E or phosphatase F, respectively. Motif B comprises a single phosphorylated substrate (S_{01} or S_{10}) as a high-affinity substrate species. In both motifs, the fast reactions that produce high-affinity species are catalyzed by enzymes that are not tightly bound to the produced high-affinity species. In Figures 2 and S2, motif A is shown in yellow with a green border, while motif B is shown in yellow with an orange border. (B) The motif structures were imposed in the parameter search by applying biased k and K_m values. The positions of imposed motifs are indicated in the diagrams below each bar chart. A rhombus divided into four subspaces represents the reaction structure shown in (A). For example, the upper left space indicates the conversion between S_{00} and S_{01} . When a green circle is shown in any of the four subspaces, motif A is imposed at the reversible phosphorylation

Figure 3. Continued

scheme corresponding to the subspace. Similarly, an orange circle denotes motif B imposed at the indicated subspace. Bar charts indicate the probability of chaotic parameter sets found in the presence of each imposed motif. In the bar charts, motif arrangements correspond to the clusters found in the random parameter search (Figures 2 and S2), which are indicated as cluster numbers. The red arrow indicates the motif arrangement with the highest probability of chaos behavior.

See also Figure S3.

symmetrical positions, while arrangements #11, #13, and #14 also exhibit higher chaos probabilities by containing two motif Bs in rotationally symmetrical positions. Second, comparisons between arrangements with only motif A or motif B show that arrangements with motif A tend to have chaos behavior more than those with motif B. Third, a certain arrangement of both motif A and motif B substantially increases the probability of chaos behavior. This is evident by comparison of the probabilities of arrangements #6, #13, and #25; all of these arrangements have motif A or B in the positions $S_{a00} \leftrightarrow S_{a01}$, $S_{a11} \leftrightarrow S_{a10}$, and $S_{b00} \leftrightarrow S_{b01}$; however, arrangement #25, which contains two motif As in substrate S_a and one motif B in substrate S_b , has a higher probability of chaos behavior than arrangements #6 and #13. It should also be noted that even if the number of included motifs increases, the inappropriate motif arrangement decreases chaos probability to a probability lower than that observed with an unbiased parameter search (e.g., arrangement #38). Among the 46 arrangements, the highest chaos probability was observed for an arrangement of S_a with two motif As in rotationally symmetrical positions and S_b with two motif Bs in rotationally symmetrical positions (arrangement #46: red arrow in Figure 3B).

With two motif As or two motif Bs in rotationally symmetrical positions, the substrate phosphorylation-dephosphorylation reaction tends to flow in a cyclic order. For example, if motif A is placed in the symmetrical positions $S_{a01} \rightarrow S_{a00}$ and $S_{a10} \rightarrow S_{a11}$ (e.g., arrangement #4), the fast dephosphorylation reaction leads to a counter-clockwise phosphorylation-dephosphorylation cycle ($S_{a01} \rightarrow S_{a00} \rightarrow S_{a10} \rightarrow S_{a11} \rightarrow S_{a01} \dots$) (see Figure 4A). This cyclical bias with stable enzyme-substrate binding is a typical motif arrangement where limit cycle oscillation occurs in a single-substrate system (Jolley et al., 2012). Accordingly, two-substrate systems with two motif As or motif Bs in rotationally symmetrical positions have a higher probability of limit cycle oscillation, as well as chaos behavior (Figure S3A). Such correlation can also be observed for other motif arrangements; for example, a motif arrangement with a high probability of chaos behavior tends to have a high probability of oscillation (Figures S3A and S3B). This relationship is to be expected, given that chaos behavior is often caused by the coupling of oscillators. However, a high probability of oscillation does not fully account for a high probability of chaos behavior because arrangement #46, which has the highest probability of chaos behavior, does not have the highest probability of oscillation (Figure S3B, red arrow). Thus, arrangement #46 retains reaction features that are important for chaos behavior.

The chaos motif arrangements create two oscillator structures

To investigate the mechanism underlying the generation of chaos behavior, we considered stereotypical chaos parameter sets ($n = 97$) based on motif arrangement #46 (Figures 3B and 4A). For comparison, we also considered stereotypical oscillation parameter sets ($n = 97$) based on motif arrangement #46. Both stereotypical parameter sets had symmetrical structures because the setting parameters in the symmetrical positions (e.g., k_{a1} and k_{a8}) had identical values.

Bifurcation analyses were performed with the stereotypical parameter sets. Bifurcation maps for stereotypical chaos sets support the importance of motif structure (Figures 4B and 4C). The motif A structure in substrate S_a is implemented by high $k_{a4/5}$ and low $K_{ma2/7}$ values. Indeed, in the bifurcation maps, chaos behavior is restricted in the range of the highest $k_{a4/5}$ and lowest $K_{ma2/7}$ values. These constraints appear to be important for avoiding the system's convergence to a fixed steady state because high $k_{a4/5}$ and low $K_{ma2/7}$ values are also critical for oscillation in the stereotypical oscillation parameter sets (Figure S4). For substrate S_b , motif B is implemented by high $k_{b1/8}$ and low $K_{mb4/6}$ values. Similar to substrate S_a , chaos behavior is restricted within the range of high $k_{b1/8}$ and low $K_{mb4/6}$ values, although this constraint appears to be less important than for motif A in substrate S_a . The importance of a motif B in substrate S_b is characteristic of chaos behavior because these parameters have a negligible impact in the bifurcation map of the stereotypical oscillation parameter sets (Figure S4). In other words, the appropriate arrangement and parameter space of both motif A in substrate S_a and motif B in substrate S_b are important for chaos behavior.

Another constraint can be found in k_{a2} . Chaos behavior and oscillation are restricted in the narrow range of $k_{a2/7}$ values (Figures 4 and S4). Indeed, $k_{a2/7}$ is critical for period determination in an oscillator composed of

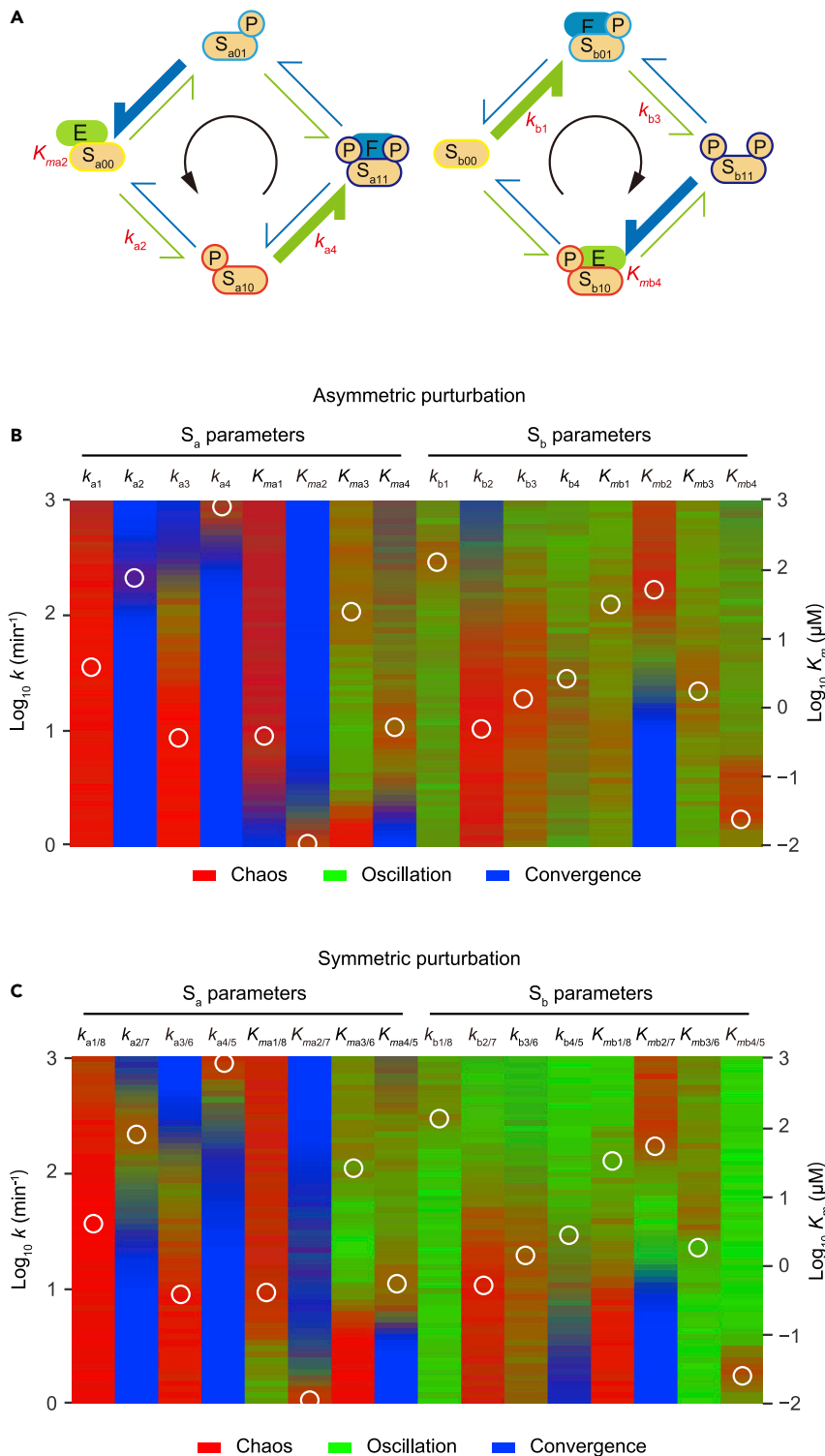


Figure 4. Critical parameters for the oscillation-chaos transition

(A) Schematic diagram of the stereotypical chaos/oscillation parameter sets.

(B) Bifurcation analysis of stereotypical chaos parameter sets ($n = 97$), all of which preserve a motif arrangement shown in the schematic representation. A heatmap shows the results of bifurcation analysis. White circles indicate the centroid of the 97 stereotypical parameter sets. The color of the heatmap represents, for a set of stereotyped parameters, the probability of chaos behavior (red), oscillation (green), or convergence to some steady state (blue) when each indicated

Figure 4. Continued

parameter is fixed to an indicated value. For example, if all 97 parameter sets had chaos behavior, the color would be red, but if half the parameter sets had chaos behavior and the other half had oscillation, the color code would be brown (50% red +50% green).

(C) The analysis method is the same as that in (B), except that the indicated parameter and its symmetrical pair (e.g., k_{a1} and k_{a8} , K_{mb4} and K_{mb5}) are simultaneously fixed to an indicated value.

See also [Figure S4](#).

a similar motif A arrangement because this rate constant determines the time required to convert all the enzyme-trapping statuses (S_{a00} and S_{a11}) to nontrapping statuses (Jolley et al., 2012). In contrast, the period-determining parameter for a motif B oscillator is $k_{b3/6}$. By comparing the parameter ranges of chaos behavior for $k_{a2/7}$ and $k_{b3/6}$ with those of an oscillation, it was found that the faster cycle (higher $k_{a2/7}$) for the S_a oscillator relative to that of the S_b oscillator appears to be important for chaos behavior. This expected period difference appears not to be important for oscillation because changes to $k_{b3/6}$ do not affect the steady-state behavior of the stereotypical oscillation parameter sets (Figure S4).

Coupling of fast and slow oscillators is raised by a combined motif A and motif B arrangement

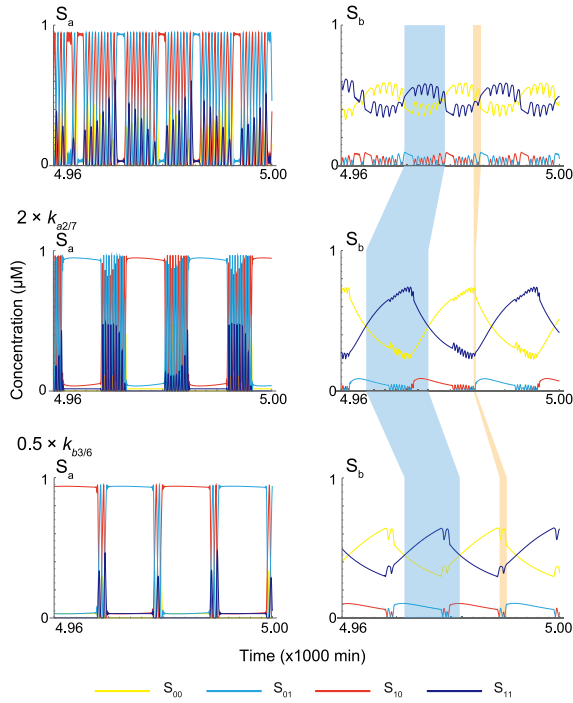
To further investigate the underlying mechanism of chaos behavior, we chose one example among the stereotypical chaos parameter sets (Table S1). The system with this example parameter set showed chaos behavior characterized by a mixture of fast and slow dynamics in the trajectory of phosphorylation statuses (Figure 5A). In Figure 5A, the approximate period of slower dynamics is shown by a blue band, whereas that of faster dynamics is shown by an orange band (see the S_b plot in Figure 5A). These short and long periods are sensitive to changes in $k_{a2/7}$ and $k_{b3/6}$ values, which are reaction parameters suggested to be critical for periods of S_a - and S_b -based oscillation (Jolley et al., 2012). A two-fold increase in $k_{a2/7}$ further shortens the short period ($2\times k_{a2/7}$: orange band in Figure 5A) while the long period is further lengthened ($2\times k_{a2/7}$: blue band in Figure 5A). On the other hand, a two-fold decrease in $k_{b3/6}$ lengthens the long period ($0.5\times k_{b3/6}$: blue band in Figure 5A) without markedly affecting the short period ($0.5\times k_{b3/6}$: orange band in Figure 5A). Because the short period is sensitive to $k_{a2/7}$, we suggest that the dynamics of substrate S_a are primarily responsible for the fast oscillatory component of chaos behavior. The slow oscillatory component may be largely determined by the coupling of S_a and S_b because both $k_{a2/7}$ and $k_{b3/6}$ affect the longer period.

The different roles of S_a and S_b were further validated by removing one of the S_a or S_b substrates from the chaos system. If the amount of S_b is set to zero with all other parameters maintained, the remaining S_a substrate shows a limit cycle oscillation with a period comparable to the fast oscillatory component of the chaos system (Figure 5B). On the other hand, if the amount of S_a is set to zero, the remaining S_b substrate shows an oscillation with a longer period than that of a S_a -only oscillation (Figure 5C). The different intrinsic periods of S_a -only and S_b -only oscillations are conserved among the stereotypical parameter sets; among the 97 stereotypical parameter sets, 85 showed oscillations in the absence of S_a or S_b . In most cases, a S_a -only oscillation had a higher frequency (i.e., shorter period) than a S_b -only oscillation (Figure 5D). The unimodal distribution of frequency difference suggests that the coupled S_a and S_b oscillators tend to behave chaotically when the frequency ratio is not too low or high. These results support the hypothesis that a S_a oscillator with an intrinsically shorter period contributes to the faster dynamics of chaos behavior and a S_b oscillator with an intrinsically longer period contributes to the slower dynamics, while the coupling between S_a and S_b dynamics is required for the slower dynamics of chaos behavior.

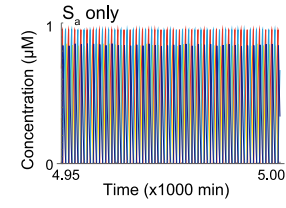
In agreement, a mixture of fast and slow dynamics was observed under increased S_a -enzyme affinity (i.e., decreased $K_{ma2/7}$) conditions (Figure S5A). Fast dynamics are absent if the affinity of the S_a -enzyme is significantly decreased (Figure S5B), suggesting that S_a -enzyme affinity is important for producing fast dynamics. In addition, increasing S_b -enzyme affinity disrupts fast dynamics (Figure S5C), while decreasing S_b -enzyme affinity disrupts slower dynamics (Figure S5D); this suggests that setting S_b -enzyme affinity at an appropriate strength is important for the coexistence of fast and slow dynamics.

The phosphorylation dynamics of S_a and S_b affect each other through the availability of a shared kinase and phosphatase. The availability of free enzymes is restricted by the presence of substrate species with high affinities to these enzymes (i.e., enzyme sequestration). Therefore, the results presented above suggest that enzyme sequestration by substrate S_a may be important for fast dynamics, whereas slower dynamics are likely related to enzyme sequestration by substrate S_b . Given this possibility, we aimed to directly visualize the behavior of a free kinase, free phosphatase, and the sequestered enzymes using a stochastic simulation (Figure 5E). This stochastic

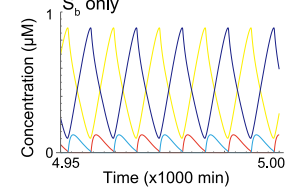
A Typical parameter set



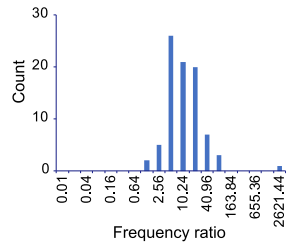
B



C



D Frequency of S_a only / S_b only



E

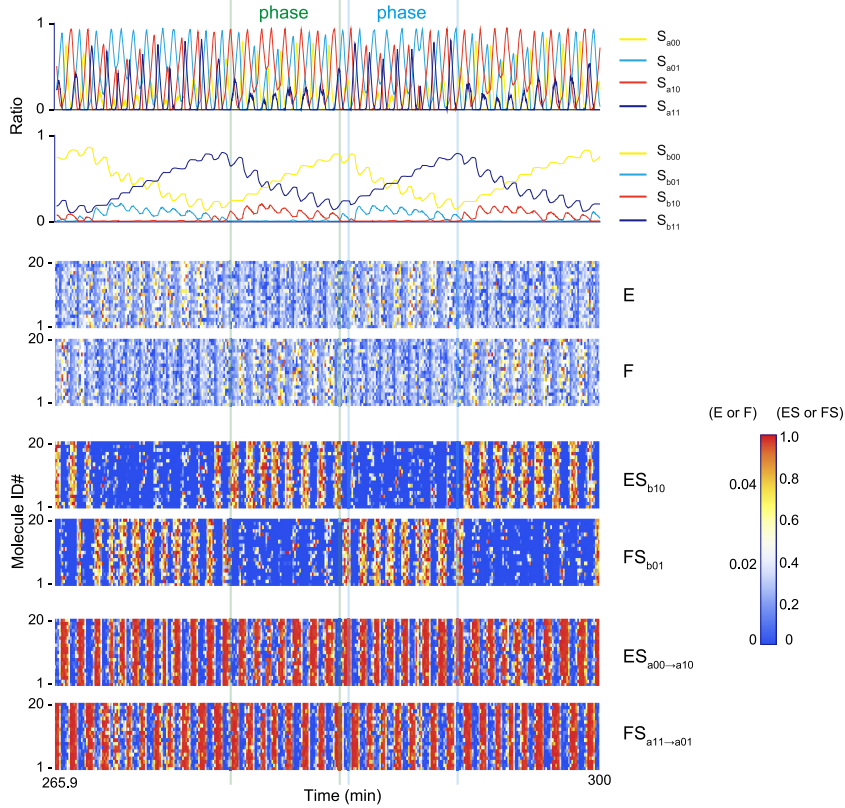


Figure 5. Dissection of timescales encoded by the chaos motifs

(A) Time course of chaotic dynamics for a representative chaos parameter set, the representative parameter set with a two-fold increase in the parameter values for symmetrical k_{a2} and k_{a7} , or the representative parameter set with a 0.5-fold decrease in the parameter values for symmetrical k_{b3} and k_{b6} . The dynamics are mainly composed of oscillatory dynamics of high and low frequency. A typical period of high-frequency oscillation is shown as an orange stripe, whereas that of a low-frequency oscillation is shown as a blue stripe.

(B) Time course of oscillatory dynamics for the representative parameter set when the amount of S_b is fixed to zero. In the absence of S_b , the parameter set gives oscillation in S_a with high frequency.

(C) Time course of oscillatory dynamics for the representative parameter set when the amount of S_a is fixed to zero. In the absence of S_a , the parameter set gives oscillation in S_b with low frequency.

(D) Comparison of frequency differences encoded by oscillatory dynamics intrinsically driven by S_a and S_b . For the 97 stereotypical chaotic parameter sets, the amount of S_a or S_b was fixed to zero. In total, 85 of the stereotypical parameter sets showed oscillation for the remaining S_b or S_a dynamics. The ratio of S_a -frequency and S_b -frequency indicates that the S_a substrate is responsible for the high-frequency oscillation in the stereotypical parameter sets.

(E) The upper two plots indicate time evolution of S_a and S_b at each phosphorylation state based on the stochastic simulation. The lower heatmaps illustrate the fraction of time that each sampled enzyme or substrate molecule (numbered as #1 to #20) spend in an indicated form (e.g., substrate-unbound free E, ES complex from $S_{b10} \rightarrow S_{b11}$) during a 0.1 s epoch. S_a molecules trap E and F reciprocally at high frequency, while S_b molecules slowly trap and release the E and F, thereby driving low-frequency rhythmicity.

See also [Figure S5](#), [Tables S1](#) and [S2](#).

simulation did not presuppose the quasi-steady-state assumption of the Michaelis-Menten reaction scheme. Instead, the dynamics of the enzyme-substrate complex were simulated explicitly. In the stochastic simulation, fast and slow dynamics were still observable in S_a and S_b phosphorylation states. Consistent with this, the availability of the free kinase (E) and free phosphatase (F) fluctuated in fast and slow dynamics. This fluctuation in the slow dynamics of E and F was represented as E-depleted and F-depleted phases, which were well matched with the presence of $ES_{b10 \rightarrow b11}$ and $FS_{b01 \rightarrow b00}$ complexes, respectively, both of which are S_b complexes with high affinities to E and F, respectively. On the other hand, $ES_{a00 \rightarrow a10}$ and $FS_{a11 \rightarrow a01}$ complexes, which are S_a complexes with high affinities to E and F, respectively, showed clear oscillations that were well matched with fast dynamics. In summary, the stochastic simulation demonstrated that enzyme sequestration by S_b species represents the slow dynamics of free enzyme availability, whereas enzyme sequestration by S_a species dominates the fast dynamics of phosphorylation statuses. The dynamics of chaos behavior may result from the coupling of S_a and S_b substrates via the availability of enzymes, which varies across timescales ([Figure 6](#)).

Discussion**Reversible phosphorylation networks in living cells**

To the best of our knowledge, this study is the first computational demonstration of a biochemical system described only by the Michaelis-Menten reaction scheme exhibiting chaos behavior. Our model can be discriminated from a set of molecular models employing the synthesis and degradation of components ([Decroly and Goldbeter, 1982](#)). Although the coupling of oscillators is understood to be one of the typical mechanisms underlying chaos generation, the model of reversible phosphorylation described by the Michaelis-Menten scheme helps connect the design principle to the possible molecular properties. We previously showed that a similar two-site phosphorylation system could be an autonomous oscillator ([Jolley et al., 2012](#)). Mathematically, the model of [Jolley et al. \(2012\)](#) is closely related to the oscillator model of KaiC protein ([Rust et al., 2007](#)), a unique cyanobacteria protein with autokinase and autophosphatase activities. Nonetheless, the model described by the generic Michaelis-Menten scheme allows us to directly compare parameter (k and K_m) combinations, leading to the theory that several kinases, including mammalian proteins, may meet the requirements for composing autonomous oscillators. The work in the present study may be similarly useful, and below we discuss how a cellular reversible phosphorylation network can be a chaos generator without the need for eccentric assumptions related to the properties of enzymes and substrates.

We employed a model with two substrates, each of which had two modification sites modified by a shared kinase and phosphatase pair. This setting includes some degree of complexity but should also be commonly observed in the phosphorylation networks of cells. A previous mass spectrometry analysis revealed that at least 75% of the complete proteome is phosphorylated ([Sharma et al., 2014](#)) and that many substrates are phosphorylated at multiple residues. On the other hand, the number of kinases and phosphatases is much smaller than the substrate variety ([Manning et al., 2002](#)). Thus, different substrates share a kinase/phosphatase pair for modification of phosphorylation residues. Kinases are also known to

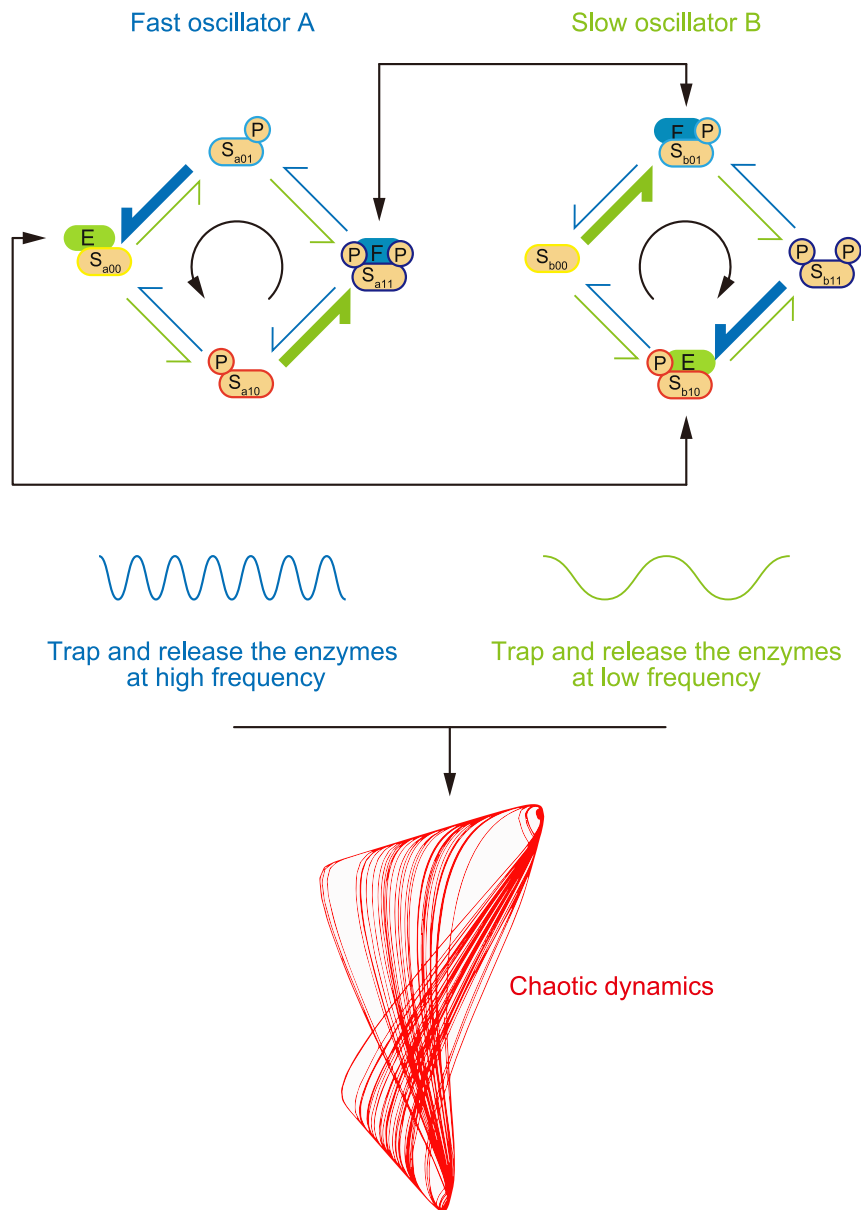


Figure 6. Coupling of posttranslational oscillators encoding different timescales

In a stereotypical arrangement of motif structure, the chaotic dynamics arise from a coupling of two-substrate modification cycles communicated by the competitive availability of shared enzymes, E and F. One substrate (S_a) intrinsically drives the reciprocal sequestration of the enzymes at high frequency, and the other substrate (S_b) intrinsically drives the enzyme sequestration at low frequency. The coupling of two such posttranslational oscillators encoding at different timescales can result in chaotic dynamics without the need for external signals or any typical allosteric regulation of enzymes.

modify a variety of non-motif substrate sequences at a different reaction rates (Miller and Turk, 2018; Ubersax and Ferrell, 2007), although kinases do have preferred substrate sequences, or consensus sequences, at which the kinase preferentially phosphorylates target residues. Therefore, a set of shared kinases and phosphatases is naturally observed in the phosphorylation network of cells.

Given this situation, it is reasonable to assume that the number of phosphorylation residues and the number of substrates sharing enzymes is greater than (and therefore more complex than) that in our model. Nevertheless, our model could be applied to more complex phosphorylation networks in which more

than two phosphorylation sites and substrate species exist. By extending the complexity of multisite phosphorylation in a substrate, it may even be possible to implement the two (distinct) substrates modeled in this study at distinct protein regions within the same substrate molecule. A similar condition can be found in phosphorylation control of the mammalian circadian protein PERIOD (PER) 2, a relatively large (~100 kDa) protein that is mostly annotated with an intrinsically disordered region (Gustafson and Partch, 2015). A previous study demonstrated that the same kinase, casein kinase I (CKI) δ/ϵ , phosphorylates at multisite phosphorylation clusters located at two distinct protein regions within PER2 (Zhou et al., 2015). Therefore, the phosphorylation of the two regions may compete with each other through different affinities to the CKI δ/ϵ kinase. Though it is currently unknown whether this circadian kinase-substrate pair exhibits autonomous chaotic phosphorylation, we expect that the phosphorylation network modeled in the present study could be implemented in a variety of molecules.

Typical chaos motifs found in actual kinases

We found that a typical chaos motif and combination of motifs had chaotic phosphorylation dynamics. Because the k and K_m values of known kinases vary by a few orders of magnitude (Bar-Even et al., 2011) and even the same kinase can show different k and K_m values depending on substrate sequences (Ubersax and Ferrell, 2007), it should be possible to identify enzyme and substrate pairs that satisfy typical chaos motifs.

The chaotic motif shown in Figure 3A requires the formation of a tight complex between the enzyme and the substrate/product. The arrangement of the motif structure with frequent occurrence of chaos behavior, as shown in Figure 2, suggests that it is important for an enzyme to modify the substrate in a specific order. These structures are common to the formation of oscillators from reversible phosphorylation (Jolley et al., 2012), and the properties required of the enzyme are also common to the formation of oscillators in several aspects. For example, CKI δ/ϵ is a candidate kinase that could achieve a chaotic motif structure. CKI δ/ϵ tightly binds to PERs and other substrate proteins (Aryal et al., 2017). Moreover, the substrate/product binding property is conserved even with short peptide substrates (Shinohara et al., 2017), which plays a role in the temperature-insensitive phosphorylation rate of this kinase. In addition, CKI δ/ϵ has a unique consensus sequence of pS-X-X-S* (pS: pre-phosphorylated serine; X: any amino acid; and S*: target serine), which allows the CKI δ/ϵ to sequentially phosphorylate the repeated S-X-X-S sequence from N- to C-terminus. Interestingly, the PER protein substrates have the repeated S-X-X-S sequence, which is known to be involved in the frequency control of circadian clock oscillation. Recent studies found that a CKI δ/ϵ isoform could phosphorylate serine at the N-terminal proximity of the S-X-X-S repeat and thereby prime for sequential phosphorylation (Fustin et al., 2018; Narasimamurthy et al., 2018). Therefore, CKI δ/ϵ and substrates with repeated S-X-X-S consensus sequences could be the building blocks for producing post-translational chaos generators. We note that sequential phosphorylation and substrate/product complex formation is also found in other kinase/substrate pairs involved in cellular signaling pathways such as cell cycle control (Miller and Turk, 2018; Valk et al., 2014).

Comparison of the posttranslational oscillator and chaos generator

Our comparisons of chaos behavior and oscillation probabilities among the various combinations of motif A and B imply that the chaos generator prefers motif A over motif B (see Figure S3B). Compared with motif A, motif B has a higher tendency to exhibit oscillation rather than chaos behavior. This is consistent with a previous study (Jolley et al., 2012), which indicated that for single-substrate systems with two reversible phosphorylation sites, a single-substrate system composed from motif B ["cluster 1" oscillator described by Jolley et al. (2012)] has a higher probability of exhibiting oscillation than that composed from motif A ["cluster 2" oscillator described by Jolley et al. (2012)].

Given that typical chaos behavior is generated by the coupled posttranslational oscillators in our system, a question arises: why is a higher chaos behavior probability derived from the presence of motif A rather than from a two-substrate system composed with motif B that shows the highest probability of oscillation? The importance of motif A for the generation of chaos behavior can be understood based on the coupling mechanism of the two substrates, which occurs through enzymatic shearing. Our stochastic simulation indicated that enzymes are trapped and released by S_b species over a slower time course (Figure 5G). To achieve enzyme trapping by S_b , it is necessary that the enzymes are released from S_a species. The S_a system shown in Figure 5 is composed of motif A (see Figure 4A for the schematic view). From this viewpoint, enzymes are released according to the oscillation process driven by motif A; focusing on kinase (E) in the S_a species, S_a is mostly trapped by the S_{a00} substrate through high kinase- S_{a00} affinity (low K_{ma2} values). The bound kinase (E) is then released from the S_{a00} when

the cyclic phosphorylation/dephosphorylation event proceeds from S_{a00} to S_{a10} . The same scenario can also be applied to the release of trapped phosphatase (F) by S_{a11} . Therefore, the trapped enzymes need to be released through the course of the (de)phosphorylation cycle. This is not the case for an oscillator composed of motif B (i.e., the S_b system in Figure 4A); the kinase (E) trapped by S_{b10} is not involved in the cyclic reaction in which S_{b10} is dephosphorylated by the phosphatase, nor is the kinase released in the course of the phosphorylation/dephosphorylation cycle. This scenario is validated by the bifurcation analysis shown in Figure 4. The kinase trapping of S_a can be very tight, as indicated by the bifurcation map in which the chaos area of K_{ma2} reaches the edge of the smallest parameter boundary ($\sim 0.01 \mu\text{M}$). Figure S5A also shows that fast and slow dynamics can persist even with a very high affinity between S_{a00} -kinase and S_{a11} -phosphatase (low $K_{ma2/7}$ values). In contrast, the kinase trapping of S_b should be tight but to a lesser extent than that of S_a ; the chaos area of K_{mb4} is within the smaller parameter range but cannot reach the smallest boundary (Figure 4). Where K_{mb4} values are too low, the enzyme may not be released from S_{b10} efficiently, and the coupling between S_a and S_b might consequently be disrupted.

In summary, although motif B is potent in exhibiting autonomous oscillation, motif A is beneficial to the coupling status of substrates with other substrate molecules through enzymatic sharing. This suggests that by combining different motif structures in different arrangements, it is possible to design biochemical networks that are suitable for generating not only oscillators that induce constant rhythms but also chaos generators that elicit spontaneous and complex dynamics in posttranslational modification.

Conclusion

Recent study demonstrated that chaos can arise from relatively simple transcriptional control models (Heltberg et al., 2019), and our study further suggests that autonomous chaos behavior can also arise from a generic mechanism of reversible multisite phosphorylation. Therefore, multisite phosphorylation networks could be sources of the spontaneous properties of cellular function, such as the stochastic nature of cellular differentiation (Furusawa and Kaneko, 2001) and the spontaneous and excitable activation of intracellular signaling observed in unicellular organisms (Devreotes et al., 2017). Thermal fluctuations in molecular activity, as well as transduction and amplification, have previously been modeled as a source of spontaneous activation in intracellular biochemical reactions (Oosawa, 2001, 2007; Ooyama and Shibata, 2011; Shibata and Ueda, 2008; Ueda and Shibata, 2007). The present study suggests that spontaneous and chaotic dynamics may also be generated from the ubiquitous setting of reversible posttranslational networks. As a similar line of research, it will also be interesting to investigate how the enzyme-substrate network avoids chaos behavior if spontaneous action leads to uncontrollable outcomes (Gelens et al., 2015).

Limitations of the study

In this study, we did not conduct an analysis of chaos system based on the analytical solution of mathematical models. Instead, we used a set of analysis based on random parameter searching, numerical integration of ordinary differential equations, and clustering analysis of chaos parameter sets. These analyses have limitations in the interpretation of the obtained results. First, although we could not find chaos in the system with single substrate having two phosphorylation sites, we cannot exclude the possibility that chaos can be observed with certain parameter combinations in the system of single substrate. Second, the mechanism of chaos generation explained in this study (e.g. Figure 6) is based on the stereotypical parameter combination illustrated as in Figure 4, and it is highly likely that there are certain parameter sets yielding chaos dynamics by the mechanism that are difficult to be categorized as "two-coupled fast and slow oscillators". Finally, since the random parameter search was performed against reversible phosphorylation models with the Michaelis-Menten approximation, the results of the random parameter search may show different trends in the distribution of the chaotic parameters if similar reversible phosphorylation systems are modeled without using the Michaelis-Menten approximation.

Resource availability

Lead contact

Further information and requests for resources should be directed to and will be fulfilled by the Lead Contact, Hiroki R. Ueda (uedah-ky@umin.ac.jp)

Materials availability

This study did not generate new unique reagents.

Data and code availability

The code generated during this study are available at GitHub https://github.com/DSP-sleep/PT_Chaotic_Oscillators.

Methods

All methods can be found in the accompanying [Transparent Methods](#) supplemental file.

Supplemental information

Supplemental Information can be found online at <https://doi.org/10.1016/j.isci.2020.101946>.

Acknowledgments

This work was supported by grants from the Brain/MINDS JP21dm0207049, Science and Technology Directorate Platform Program for Advanced Biological Medicine JP21am0401011, AMED-CREST JP21gm0610006 (AMED/MEXT) (H.R.U.), Grant-in-Aid for Scientific Research (S) JP25221004 (JSPS KAKENHI) (H.R.U.) and Scientific Research (C) JP20K06576 (JSPS KAKENHI) (K.L.O.), HFSP Research Grant Program RGP0019/2018 (HFSP) (H.R.U.), ERATO JPMJER2001 (JST) (H.R.U.) and an intramural Grant-in-Aid from the RIKEN BDR (H.R.U.). The authors would like to thank Enago (www.enago.jp) for the English language review.

Author contributions

H.Q.Y., K.L.O., and H.R.U. designed the study. H.Q.Y. performed most of the simulation study. H.Q.Y., K.L.O., and H.R.U. analyzed the mechanism of chaos generation and wrote the manuscript.

Declaration of interests

H.R.U. is a member of the iScience's editorial advisory board.

Received: October 5, 2020

Revised: December 2, 2020

Accepted: December 11, 2020

Published: January 22, 2021

References

- Aihara, K., Matsumoto, G., and Ichikawa, M. (1985). An alternating periodic-chaotic sequence observed in neural oscillators. *Phys. Lett. A* *111*, 251–255.
- Aryal, R.P., Kwak, P.B., Tamayo, A.G., Gebert, M., Chiu, P.L., Walz, T., and Weitz, C.J. (2017). Macromolecular assemblies of the mammalian circadian clock. *Mol. Cell* *67*, 770–782 e776.
- Bar-Even, A., Noor, E., Savir, Y., Liebermeister, W., Davidi, D., Tawfik, D.S., and Milo, R. (2011). The moderately efficient enzyme: evolutionary and physicochemical trends shaping enzyme parameters. *Biochemistry* *50*, 4402–4410.
- Bieler, J., Cannavo, R., Gustafson, K., Gobet, C., Gatfield, D., and Naef, F. (2014). Robust synchronization of coupled circadian and cell cycle oscillators in single mammalian cells. *Mol. Syst. Biol.* *10*, 739.
- Chen, Z., Kibler, R.D., Hunt, A., Busch, F., Pearl, J., Jia, M., VanAernum, Z.L., Wicky, B.I.M., Dods, G., Liao, H., et al. (2020). De novo design of protein logic gates. *Science* *368*, 78–84.
- Chickarmane, V., Kholodenko, B.N., and Sauro, H.M. (2007). Oscillatory dynamics arising from competitive inhibition and multisite phosphorylation. *J. Theor. Biol.* *244*, 68–76.
- Conradi, C., Mincheva, M., and Shiu, A. (2019). Emergence of oscillations in a mixed-mechanism phosphorylation system. *Bull. Math. Biol.* *81*, 1829–1852.
- Conradi, C., and Shiu, A. (2018). Dynamics of posttranslational modification systems: recent progress and future directions. *Biophysical J.* *114*, 507–515.
- Decroly, O., and Goldbeter, A. (1982). Birhythmicity, chaos, and other patterns of temporal self-organization in a multiply regulated biochemical system. *Proc. Natl. Acad. Sci. U S A* *79*, 6917–6921.
- Devreotes, P.N., Bhattacharya, S., Edwards, M., Iglesias, P.A., Lampert, T., and Miao, Y. (2017). Excitable signal transduction networks in directed cell migration. *Annu. Rev. Cell Dev. Biol.* *33*, 103–125.
- Durston, A.J. (1974). Pacemaker mutants of *Dictyostelium discoideum*. *Dev. Biol.* *38*, 308–319.
- Fink, T., Lonzaric, J., Praznik, A., Plaper, T., Merljak, E., Leben, K., Jerala, N., Lebar, T., Strmsek, Z., Lapenta, F., et al. (2019). Design of fast proteolysis-based signaling and logic circuits in mammalian cells. *Nat. Chem. Biol.* *15*, 115–122.
- Furusawa, C., and Kaneko, K. (2001). Theory of robustness of irreversible differentiation in a stem cell system: chaos hypothesis. *J. Theor. Biol.* *209*, 395–416.
- Fustin, J.M., Kojima, R., Itoh, K., Chang, H.Y., Ye, S., Zhuang, B., Oji, A., Gibo, S., Narasimamurthy, R., Virshup, D., et al. (2018). Two Ck1delta transcripts regulated by m6A methylation code for two antagonistic kinases in the control of the circadian clock. *Proc. Natl. Acad. Sci. U S A* *115*, 5980–5985.
- Gao, X.J., Chong, L.S., Kim, M.S., and Elowitz, M.B. (2018). Programmable protein circuits in living cells. *Science* *361*, 1252–1258.
- Gelens, L., Huang, K.C., and Ferrell, J.E., Jr. (2015). How does the *Xenopus laevis* embryonic cell cycle avoid spatial chaos? *Cell Rep.* *12*, 892–900.
- Gerard, C., and Goldbeter, A. (2012). Entrainment of the mammalian cell cycle by the circadian clock: modeling two coupled cellular rhythms. *PLoS Comput. Biol.* *8*, e1002516.

- Goldbeter, A. (2002). Computational approaches to cellular rhythms. *Nature* 420, 238–245.
- Gustafson, C.L., and Partch, C.L. (2015). Emerging models for the molecular basis of mammalian circadian timing. *Biochemistry* 54, 134–149.
- Heltberg, M.L., Krishna, S., and Jensen, M.H. (2019). On chaotic dynamics in transcription factors and the associated effects in differential gene regulation. *Nat. Commun.* 10, 71.
- Izhikevich, E.M. (2007). *Dynamical Systems in Neuroscience* (MIT Press).
- Jolley, C.C., Ode, K.L., and Ueda, H.R. (2012). A design principle for a posttranslational biochemical oscillator. *Cell Rep.* 2, 938–950.
- Kauffman, S.A. (1992). Origins of order in evolution: self-organization and Selection. In *Understanding Origins: Contemporary Views on the Origin of Life, Mind and Society*, F.J. Varela and J.-P. Dupuy, eds. (Springer Netherlands), pp. 153–181.
- Kholodenko, B.N. (2006). Cell-signalling dynamics in time and space. *Nat. Rev. Mol. Cell Biol.* 7, 165–176.
- Langton, C.G. (1990). Computation at the edge of chaos: phase transitions and emergent computation. *Physica D Nonlinear Phenomena* 42, 12–37.
- Liu, P., Kevrekidis, I.G., and Shvartsman, S.Y. (2011). Substrate-dependent control of ERK phosphorylation can lead to oscillations. *Biophysical J.* 101, 2572–2581.
- Manning, G., Whyte, D.B., Martinez, R., Hunter, T., and Sudarsanam, S. (2002). The protein kinase complement of the human genome. *Science* 298, 1912–1934.
- Markevich, N.I., Hoek, J.B., and Kholodenko, B.N. (2004). Signaling switches and bistability arising from multisite phosphorylation in protein kinase cascades. *J. Cell Biol.* 164, 353–359.
- Markevich, N.I., Tsyanov, M.A., Hoek, J.B., and Kholodenko, B.N. (2006). Long-range signaling by phosphoprotein waves arising from bistability in protein kinase cascades. *Mol. Syst. Biol.* 2, 61.
- Martiel, J.L., and Goldbeter, A. (1985). Autonomous chaotic behaviour of the slime mould *Dictyostelium discoideum* predicted by a model for cyclic AMP signalling. *Nature* 313, 590–592.
- Matsuo, T., Yamaguchi, S., Mitsui, S., Emi, A., Shimoda, F., and Okamura, H. (2003). Control mechanism of the circadian clock for timing of cell division in vivo. *Science* 302, 255–259.
- Miller, C.J., and Turk, B.E. (2018). Homing in: mechanisms of substrate targeting by protein kinases. *Trends Biochem. Sci.* 43, 380–394.
- Murray, A.W., and Kirschner, M.W. (1989). Cyclin synthesis drives the early embryonic cell cycle. *Nature* 339, 275–280.
- Nagoshi, E., Saini, C., Bauer, C., Laroche, T., Naef, F., and Schibler, U. (2004). Circadian gene expression in individual fibroblasts: cell-autonomous and self-sustained oscillators pass time to daughter cells. *Cell* 119, 693–705.
- Narasimamurthy, R., Hunt, S.R., Lu, Y., Fustin, J.M., Okamura, H., Partch, C.L., Forger, D.B., Kim, J.K., and Virshup, D.M. (2018). CK1delta/epsilon protein kinase primes the PER2 circadian phosphoswitch. *Proc. Natl. Acad. Sci. U S A* 115, 5986–5991.
- Olsen, L.F., and Degn, H. (1977). Chaos in an enzyme reaction. *Nature* 267, 177–178.
- Oosawa, F. (2001). Spontaneous signal generation in living cells. *Bull. Math. Biol.* 63, 643–654.
- Oosawa, F. (2007). Spontaneous activity of living cells. *Bio Syst.* 88, 191–201.
- Ooyama, S., and Shibata, T. (2011). Hierarchical organization of noise generates spontaneous signal in *Paramecium* cell. *J. Theor. Biol.* 283, 1–9.
- Palmeirim, I., Henrique, D., Ish-Horowicz, D., and Pourquie, O. (1997). Avian hairy gene expression identifies a molecular clock linked to vertebrate segmentation and somitogenesis. *Cell* 91, 639–648.
- Pomerening, J.R., Kim, S.Y., and Ferrell, J.E., Jr. (2005). Systems-level dissection of the cell-cycle oscillator: bypassing positive feedback produces damped oscillations. *Cell* 122, 565–578.
- Pomerening, J.R., Sontag, E.D., and Ferrell, J.E., Jr. (2003). Building a cell cycle oscillator: hysteresis and bistability in the activation of *Cdc2*. *Nat. Cell Biol.* 5, 346–351.
- Qiao, L., Nachbar, R.B., Kevrekidis, I.G., and Shvartsman, S.Y. (2007). Bistability and oscillations in the Huang-Ferrell model of MAPK signaling. *PLoS Comput. Biol.* 3, 1819–1826.
- Raskin, D.M., and de Boer, P.A. (1999). Rapid pole-to-pole oscillation of a protein required for directing division to the middle of *Escherichia coli*. *Proc. Natl. Acad. Sci. U S A* 96, 4971–4976.
- Rasmussen, R., Jensen, M.H., and Heltberg, M.L. (2017). Chaotic dynamics mediate Brain state transitions, driven by changes in extracellular ion concentrations. *Cell Syst.* 5, 591–603 e594.
- Rust, M.J., Markson, J.S., Lane, W.S., Fisher, D.S., and O’Shea, E.K. (2007). Ordered phosphorylation governs oscillation of a three-protein circadian clock. *Science* 318, 809–812.
- Shankaran, H., Ippolito, D.L., Chrisler, W.B., Resat, H., Bollinger, N., Opresko, L.K., and Wiley, H.S. (2009). Rapid and sustained nuclear-cytoplasmic ERK oscillations induced by epidermal growth factor. *Mol. Syst. Biol.* 5, 332.
- Sharma, K., D’Souza, R.C., Tyanova, S., Schaab, C., Wisniewski, J.R., Cox, J., and Mann, M. (2014). Ultradeep human phosphoproteome reveals a distinct regulatory nature of Tyr and Ser/Thr-based signaling. *Cell Rep.* 8, 1583–1594.
- Shibata, T., and Ueda, M. (2008). Noise generation, amplification and propagation in chemotactic signaling systems of living cells. *Bio Syst.* 93, 126–132.
- Shinohara, Y., Koyama, Y.M., Ukai-Tadenuma, M., Hirokawa, T., Kikuchi, M., Yamada, R.G., Ukai, H., Fujishima, H., Umehara, T., Tainaka, K., et al. (2017). Temperature-sensitive substrate and product binding underlie temperature-compensated phosphorylation in the clock. *Mol. Cell* 67, 783–798 e720.
- Skarda, C.A., and Freeman, W.J. (1987). How brains make chaos in order to make sense of the world. *Behav. Brain Sci.* 10, 161–173.
- Strogatz, S.H. (1994). *Nonlinear Dynamics and Chaos: With Applications to Physics, Biology, Chemistry, and Engineering* (Reading, Mass (Addison-Wesley Pub.)).
- Sugai, S.S., Ode, K.L., and Ueda, H.R. (2017). A design principle for an autonomous post-translational pattern formation. *Cell Rep.* 19, 863–874.
- Suwanmajo, T., and Krishnan, J. (2015). Mixed mechanisms of multi-site phosphorylation. *J. R. Soc. Interface* 12, 20141405.
- Thomson, M., and Gunawardena, J. (2009). Unlimited multistability in multisite phosphorylation systems. *Nature* 460, 274–277.
- Ubersax, J.A., and Ferrell, J.E., Jr. (2007). Mechanisms of specificity in protein phosphorylation. *Nat. Rev. Mol. Cell Biol.* 8, 530–541.
- Ueda, M., and Shibata, T. (2007). Stochastic signal processing and transduction in chemotactic response of eukaryotic cells. *Biophysical J.* 93, 11–20.
- Valk, E., Venta, R., Ord, M., Faustova, I., Koivomagi, M., and Loog, M. (2014). Multistep phosphorylation systems: tunable components of biological signaling circuits. *Mol. Biol. Cell* 25, 3456–3460.
- Yan, J., and Goldbeter, A. (2019a). Multi-rhythmicity generated by coupling two cellular rhythms. *J. R. Soc. Interface* 16, 20180835.
- Yan, J., and Goldbeter, A. (2019b). Robust synchronization of the cell cycle and the circadian clock through bidirectional coupling. *J. R. Soc. Interface* 16, 20190376.
- Yang, Q., Pando, B.F., Dong, G., Golden, S.S., and van Oudenaarden, A. (2010). Circadian gating of the cell cycle revealed in single cyanobacterial cells. *Science* 327, 1522–1526.
- Yoshioka-Kobayashi, K., Matsumiya, M., Niino, Y., Isomura, A., Kori, H., Miyawaki, A., and Kageyama, R. (2020). Coupling delay controls synchronized oscillation in the segmentation clock. *Nature* 580, 119–123.
- Zhou, M., Kim, J.K., Eng, G.W., Forger, D.B., and Virshup, D.M. (2015). A Period2 phosphoswitch regulates and temperature compensates circadian period. *Mol. Cell* 60, 77–88.

iScience, Volume 24

Supplemental Information

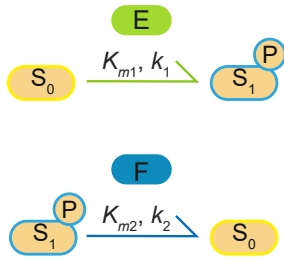
A design principle for posttranslational chaotic oscillators

Hiroto Q. Yamaguchi, Koji L. Ode, and Hiroki R. Ueda

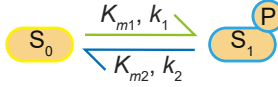
Supplemental Figures

A

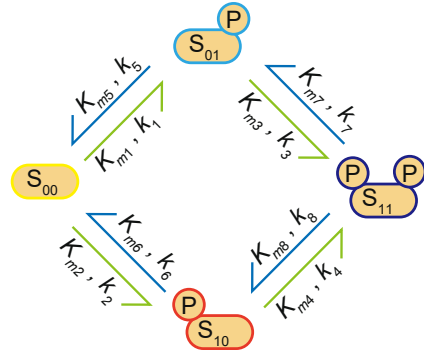
Kinase and phosphatase reactions



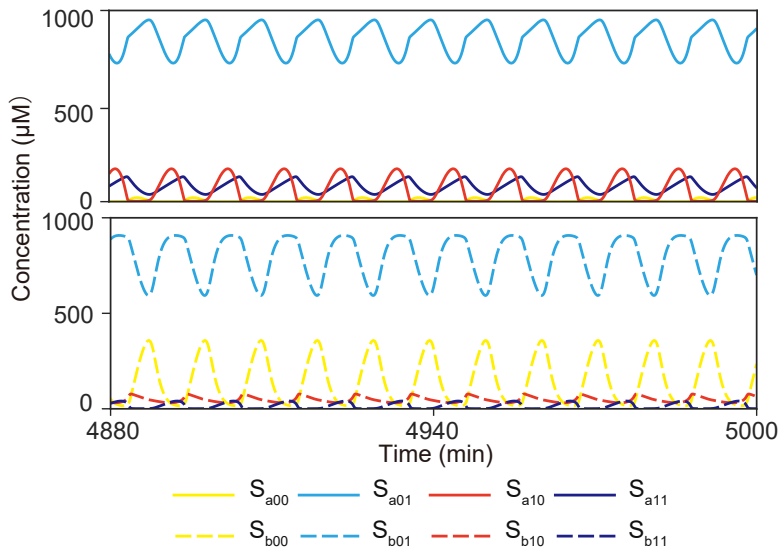
Reversible phosphorylation of single substrate with one phosphorylation site



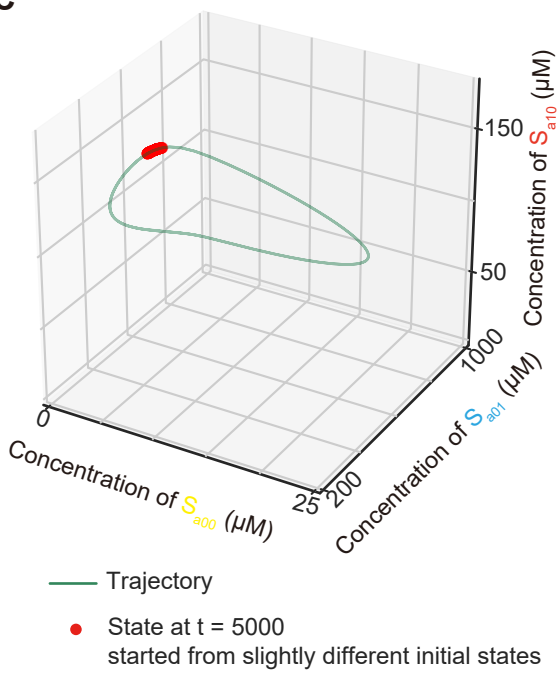
Reversible phosphorylation of single substrate with two phosphorylation sites



B



C



D

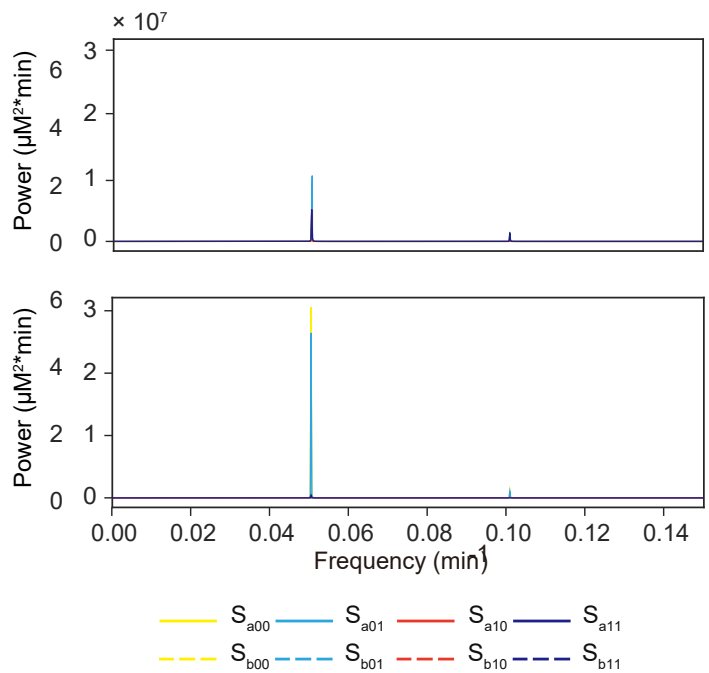


Figure S1. Yamaguchi et al.

Figure S1. Oscillatory behavior of a coupled dual-phosphorylation system

(A) Scheme of reversible phosphorylation models.

(B) An example time course of oscillatory phosphorylation dynamics.

(C) The example oscillatory dynamics of $t = 0$ min to $t = 5,000$ min are projected to S_{a00} - S_{a01} - S_{a10} space (green line). Red dots indicate the phosphorylation states at $t = 5,000$ min obtained from 200 runs of the simulation with slightly different initial conditions.

(D) Power spectrum of the example oscillatory trajectory analyzed by FFT.

See also **Figure 1**.

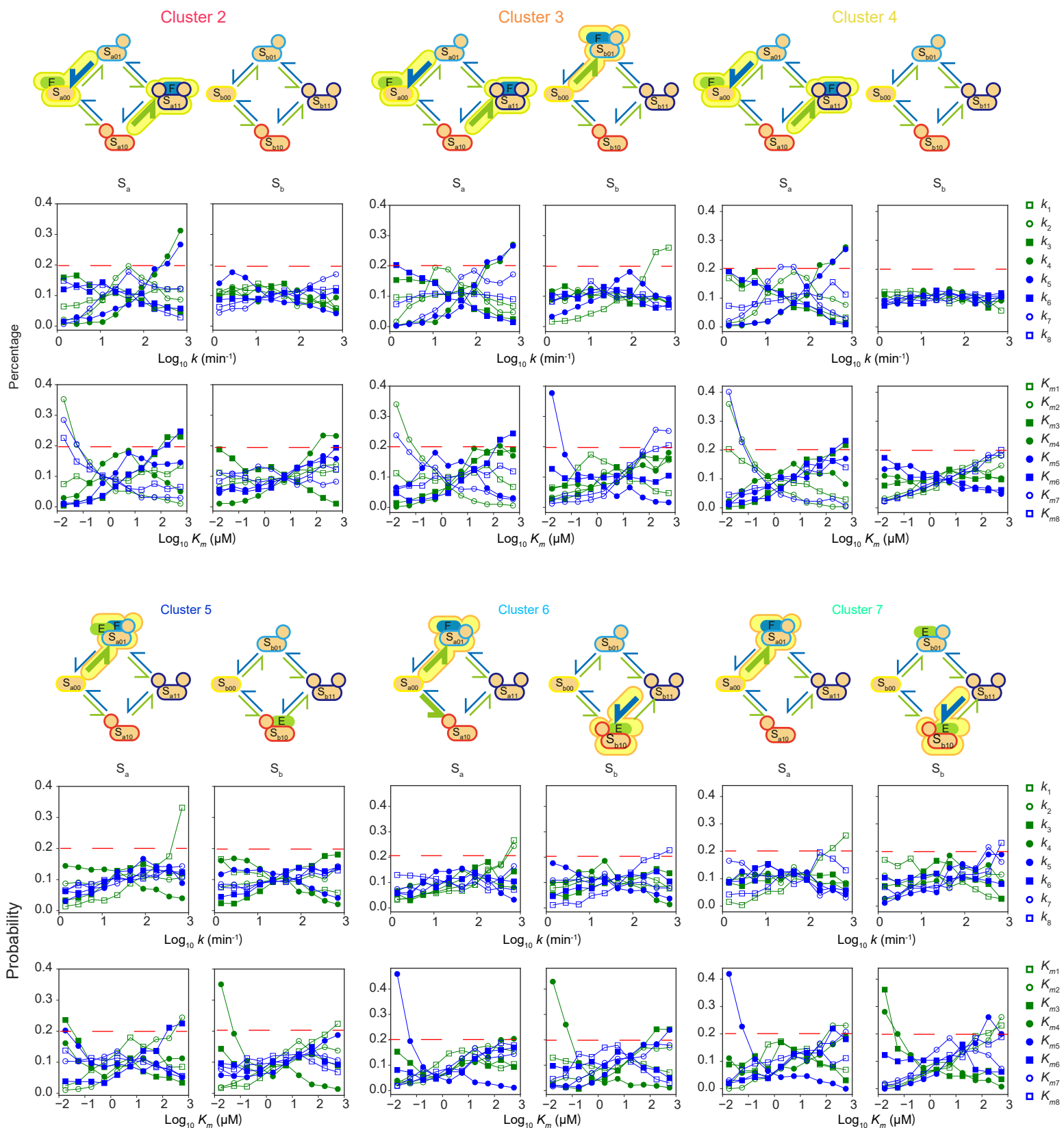


Figure S2. Yamaguchi et al.

Figure S2. Parameter motifs found in chaotic parameter sets

Schematic representation and parameter histograms of the chaotic parameter clusters shown in the same manner as in **Figure 2**.

See also **Figure 2**.

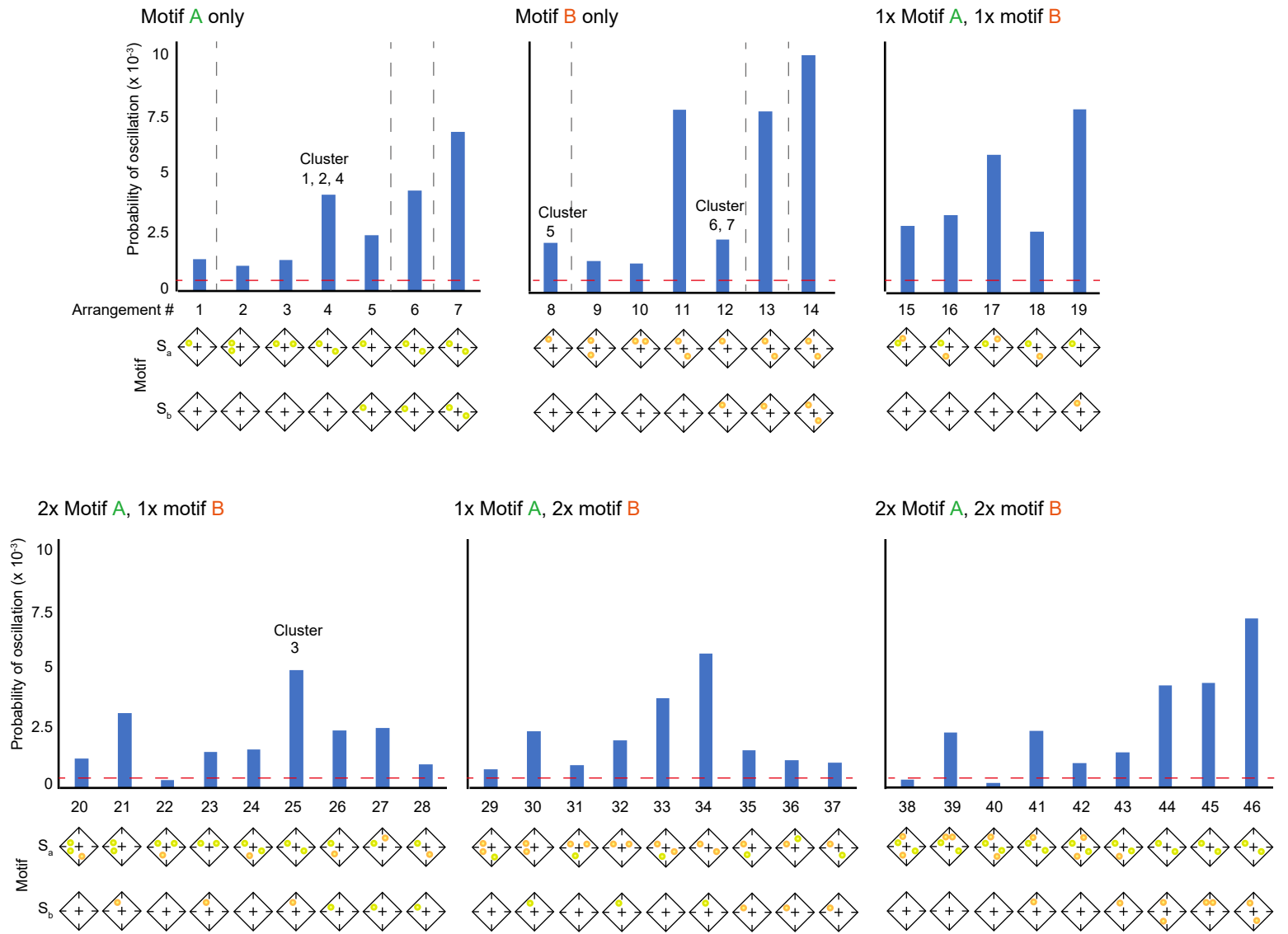
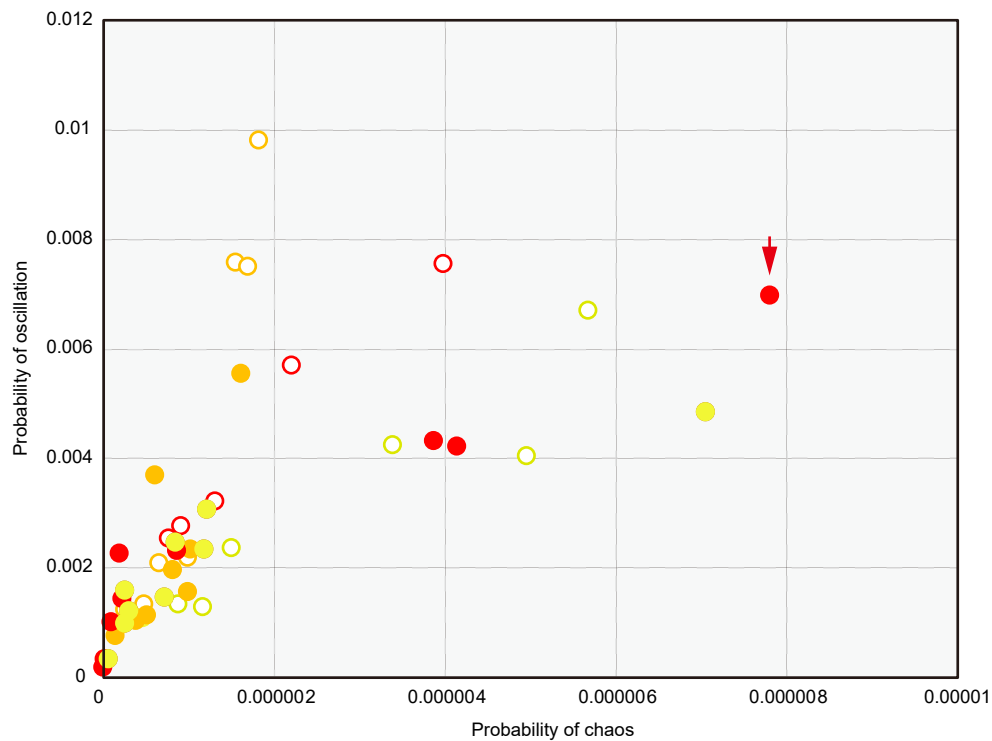
A**B**

Figure S3. Yamaguchi et al.

Figure S3. Specific arrangements of motif structure are important for chaos generation

(A) Bar charts indicate the probability of oscillatory parameter sets found in the presence of each imposed motif. Imposed motif arrangements are shown in the same manner as in **Figure 3**.

(B) A comparison of the probability of chaos behavior and oscillation for parameters in the presence of each combination of imposed motifs. The red arrow indicates the motif arrangement with the highest probability of chaos behavior (i.e., arrangement #46).

See also **Figure 3**.

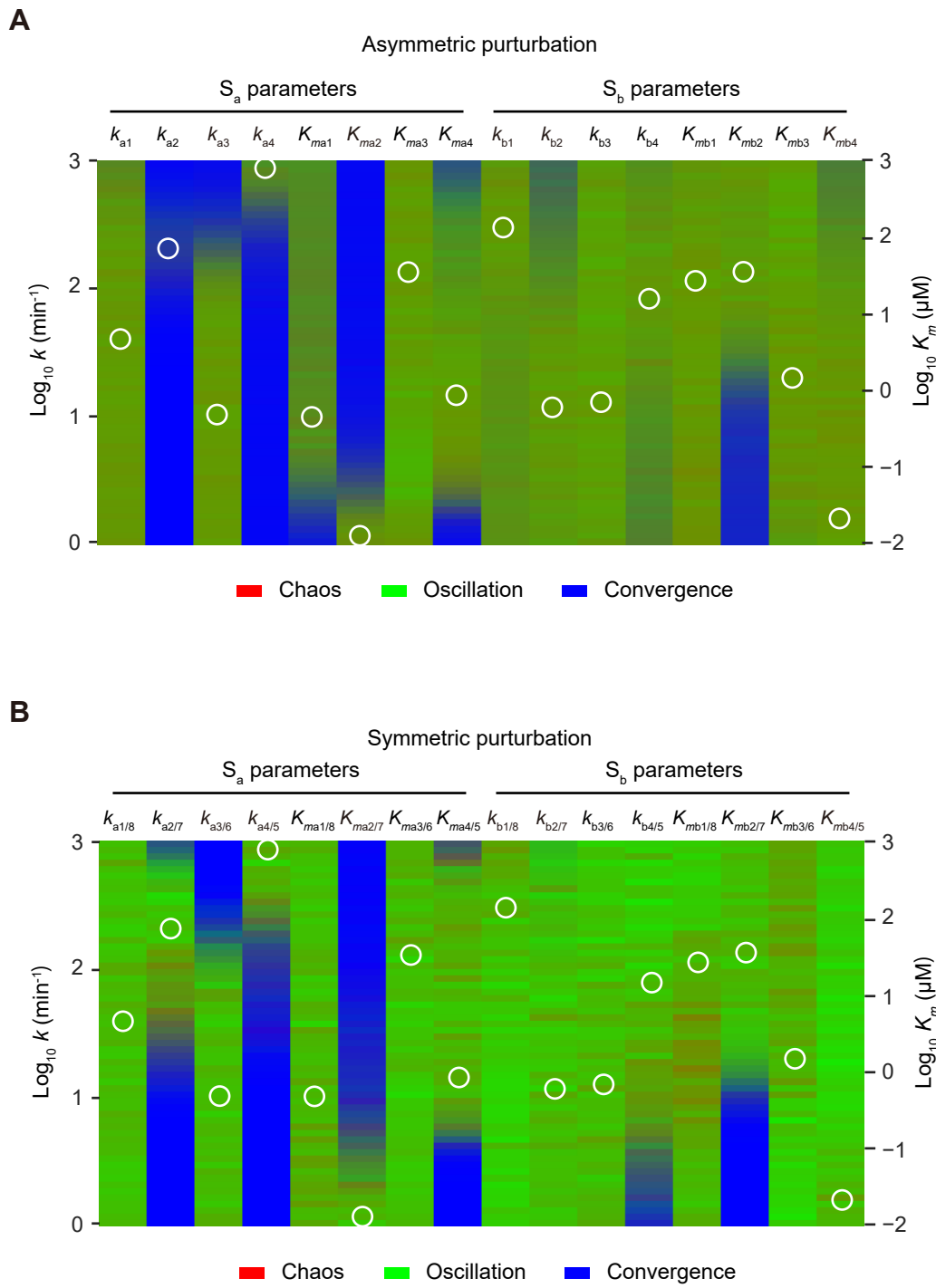


Figure S4. Yamaguchi et al.

Figure S4. Bifurcation analysis of stereotypical oscillation parameter sets.

(A) Bifurcation analysis was conducted for stereotypical oscillatory parameter sets ($n = 97$), all of which preserve the motif arrangement shown in the schematic representation in (A). The method used is same as that reported in **Figure 4B**.

(B) The same analysis as that in (A) is shown, except that the indicated parameter and its symmetrical pair (e.g., k_{a1} and k_{a8} , K_{mb4} and K_{mb5}) are simultaneously fixed to an indicated value.

See also **Figure 4**.

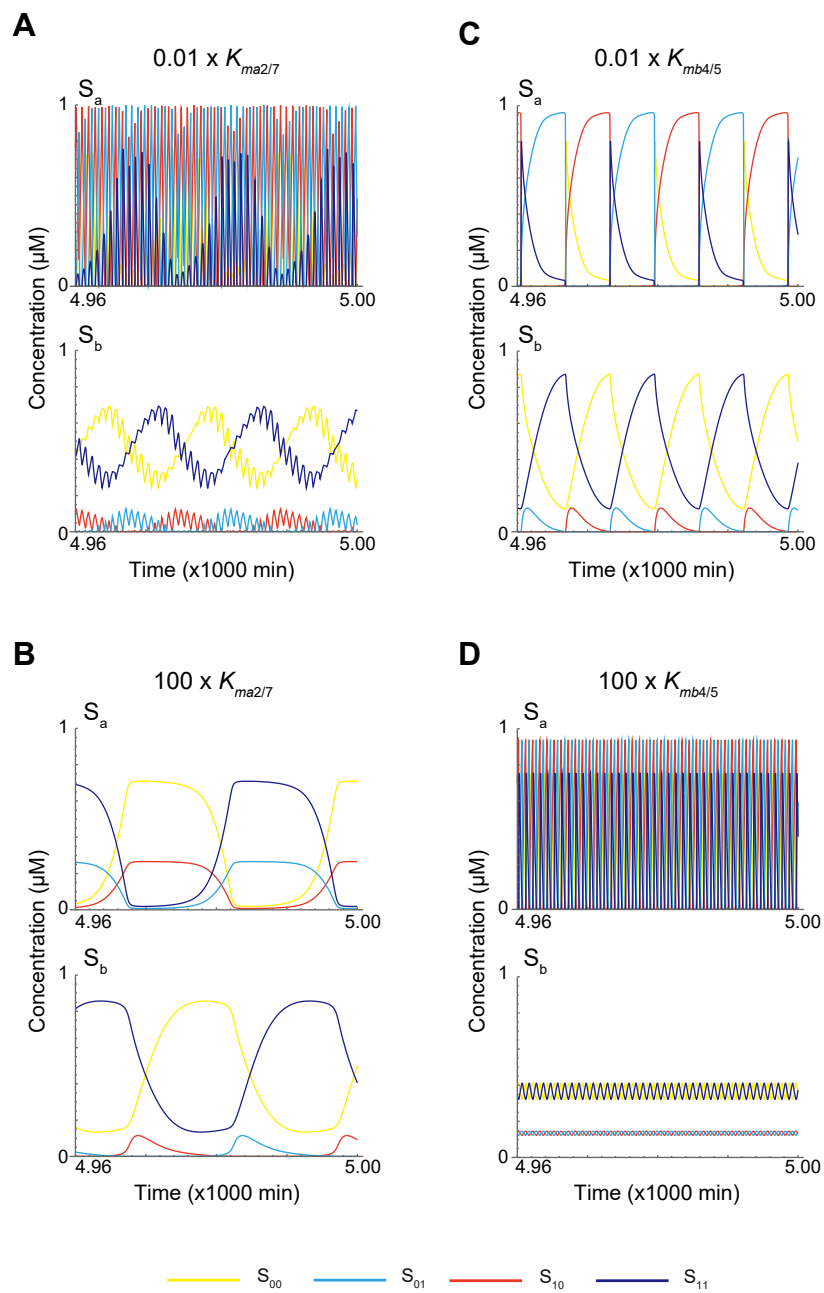


Figure S5. Yamaguchi et al.

Figure S5. Roles of enzyme trap efficiency in the coupling of two oscillators

(A, B) Time course of oscillatory dynamics for the representative parameter set with a 0.01-fold decrease (A) or 100-fold increase (B) in the parameter values for symmetrical K_{ma2} and K_{ma7} . Increasing the enzyme sequestration efficiency by S_a substrate (A) did not severely affect chaotic dynamics; reducing the enzyme sequestration by S_a (B) only allowed S_b -sequestration to drive the rhythmic synchronization of phosphorylation states such that the entire dynamics became dominated by slow-frequency oscillation.

(C, D) Time course of oscillatory dynamics for the representative parameter set with a 0.01-fold decrease (C) or 100-fold increase (D) in the parameter values for symmetrical K_{mb4} and K_{mb5} . Increasing the enzyme sequestration efficiency by S_b substrate (C) masked the high-frequency rhythmicity driven by S_a ; reducing the enzyme sequestration by S_b (D) only allowed S_a -sequestration to drive the rhythmic synchronization of phosphorylation states such that the entire dynamics became dominated by high-frequency oscillation.

Supplemental Tables

Table S1. Example stereotypical chaos parameter set, related to **Figure 5**.

Parameter k (min^{-1}), K_m (μM)	Example stereotypical chaos parameter set
k_{a1}	47.24854606
k_{a2}	103.9531911
k_{a3}	10.08171512
k_{a4}	1060.571158
k_{a5}	1060.571158
k_{a6}	10.08171512
k_{a7}	103.9531911
k_{a8}	47.24854606
K_{ma1}	1.471248283
K_{ma2}	0.008378714
K_{ma3}	57.41102352
K_{ma4}	2.597629575
K_{ma5}	2.597629575
K_{ma6}	57.41102352
K_{ma7}	0.008378714
K_{ma8}	1.471248283
k_{b1}	209.3650037
k_{b2}	10.6326728
k_{b3}	19.66831864
k_{b4}	12.42448634
k_{b5}	12.42448634
k_{b6}	19.66831864
k_{b7}	10.6326728
k_{b8}	209.3650037
K_{mb1}	87.77317768
K_{mb2}	38.41198729
K_{mb3}	4.314899945
K_{mb4}	0.04746365
K_{mb5}	0.04746365
K_{mb6}	4.314899945
K_{mb7}	38.41198729
K_{mb8}	87.77317768

Table S2. Example stereotypical chaos parameter set for stochastic simulation, related to **Figure 5**.

Parameter k (min^{-1}), k_c ($\text{min}^{-1} \mu\text{M}^{-1}$), k_{uc} (min^{-1})	Example stereotypical chaos parameter set (stochastic simulation)
k_{a1}	47.24854606
k_{a2}	103.9531911
k_{a3}	10.08171512
k_{a4}	1060.571158
k_{a5}	1060.571158
k_{a6}	10.08171512
k_{a7}	103.9531911
k_{a8}	47.24854606
$k_{uca1} - k_{uca8}$	10
k_{ca1}	32.794
k_{ca2}	12526
k_{ca3}	0.19302
k_{ca4}	408.67
k_{ca5}	408.67
k_{ca6}	0.19302
k_{ca7}	12526
k_{ca8}	32.794
k_{b1}	209.3650037
k_{b2}	10.6326728
k_{b3}	19.66831864
k_{b4}	12.42448634
k_{b5}	12.42448634
k_{b6}	19.66831864
k_{b7}	10.6326728
k_{b8}	209.3650037
$k_{ucb1} - k_{ucb8}$	10
k_{cb1}	2.3967
k_{cb2}	0.30284
k_{cb3}	4.79
k_{cb4}	282.84
k_{cb5}	282.84
k_{cb6}	4.79
k_{cb7}	0.30284
k_{cb8}	2.3967

Transparent Methods

Modeling of coupled-posttranslational oscillator system

The coupled-posttranslational oscillator system was formulated as a set of ten ordinary differential equations that describe the temporal evolution of the concentrations of eight substrate phosphorylation states and two unbound enzymes.

$$\frac{d[S_{a00}]}{dt} = -\left(\frac{k_{a1}}{K_{ma1}} + \frac{k_{a2}}{K_{ma2}}\right) [E][S_{a00}] + \left(\frac{k_{a5}}{K_{ma5}} [S_{a01}] + \frac{k_{a6}}{K_{ma6}} [S_{a10}]\right) [F] \quad (1)$$

$$\frac{d[S_{a01}]}{dt} = \left(\frac{k_{a1}}{K_{ma1}} [S_{a00}] - \frac{k_{a3}}{K_{ma3}} [S_{a01}]\right) [E] + \left(-\frac{k_{a5}}{K_{ma5}} [S_{a01}] + \frac{k_{a7}}{K_{ma7}} [S_{a11}]\right) [F] \quad (2)$$

$$\frac{d[S_{a10}]}{dt} = \left(\frac{k_{a2}}{K_{ma2}} [S_{a00}] - \frac{k_{a4}}{K_{ma4}} [S_{a10}]\right) [E] + \left(-\frac{k_{a6}}{K_{ma6}} [S_{a10}] + \frac{k_{a8}}{K_{ma8}} [S_{a11}]\right) [F] \quad (3)$$

$$\frac{d[S_{a11}]}{dt} = \left(\frac{k_{a3}}{K_{ma3}} [S_{a01}] + \frac{k_{a4}}{K_{ma4}} [S_{a10}]\right) [E] - \left(\frac{k_{a6}}{K_{ma6}} + \frac{k_{a8}}{K_{ma8}}\right) [F][S_{a11}] \quad (4)$$

$$\frac{d[S_{b00}]}{dt} = -\left(\frac{k_{b1}}{K_{mb1}} + \frac{k_{b2}}{K_{mb2}}\right) [E][S_{b00}] + \left(\frac{k_{b5}}{K_{mb5}} [S_{b01}] + \frac{k_{b6}}{K_{mb6}} [S_{b10}]\right) [F] \quad (5)$$

$$\frac{d[S_{b01}]}{dt} = \left(\frac{k_{b1}}{K_{mb1}} [S_{b00}] - \frac{k_{b3}}{K_{mb3}} [S_{b01}]\right) [E] + \left(-\frac{k_{b5}}{K_{mb5}} [S_{b01}] + \frac{k_{b7}}{K_{mb7}} [S_{b11}]\right) [F] \quad (6)$$

$$\frac{d[S_{b10}]}{dt} = \left(\frac{k_{b2}}{K_{mb2}} [S_{b00}] - \frac{k_{b4}}{K_{mb4}} [S_{b10}]\right) [E] + \left(-\frac{k_{b6}}{K_{mb6}} [S_{b10}] + \frac{k_{b8}}{K_{mb8}} [S_{b11}]\right) \quad (7)$$

$$\frac{d[S_{b11}]}{dt} = \left(\frac{k_{b3}}{K_{mb3}} [S_{b01}] + \frac{k_{b4}}{K_{mb4}} [S_{b10}]\right) [E] - \left(\frac{k_{b6}}{K_{mb6}} + \frac{k_{b8}}{K_{mb8}}\right) [F][S_{b11}] \quad (8)$$

$$[E] = \frac{E_{\text{total}}}{1 + \frac{[S_{a00}]}{K_{ma1}} + \frac{[S_{a00}]}{K_{ma2}} + \frac{[S_{a01}]}{K_{ma3}} + \frac{[S_{a10}]}{K_{ma4}} + \frac{[S_{b00}]}{K_{mb1}} + \frac{[S_{b01}]}{K_{mb2}} + \frac{[S_{b10}]}{K_{mb3}} + \frac{[S_{b10}]}{K_{mb4}}} \quad (9)$$

$$[F] = \frac{F_{\text{total}}}{1 + \frac{[S_{a01}]}{K_{ma5}} + \frac{[S_{a10}]}{K_{ma6}} + \frac{[S_{a11}]}{K_{ma7}} + \frac{[S_{a11}]}{K_{ma8}} + \frac{[S_{b01}]}{K_{mb5}} + \frac{[S_{b10}]}{K_{mb6}} + \frac{[S_{b11}]}{K_{mb7}} + \frac{[S_{b11}]}{K_{mb8}}} \quad (10)$$

In these equations, $[S_{a00}]$, $[S_{a01}]$, $[S_{a10}]$, and $[S_{a11}]$ represent the concentrations of the four phosphorylation states of substrate A; $[S_{b00}]$, $[S_{b01}]$, $[S_{b10}]$, and $[S_{b11}]$ represent the concentrations of the four phosphorylation states of substrate B; $[E]$ and $[F]$ are the concentrations of free (unbound) kinase and phosphatase; k_{a1} - k_{a8} and k_{b1} - k_{b8} are the reaction rate constants; K_{ma1} - K_{ma8} and K_{mb1} - K_{mb8} are the Michaelis-Menten constants; and E_{total} and F_{total} are the total concentrations of kinase and phosphatase.

Random parameter search for chaotic and oscillatory parameter sets

We randomly generated parameter sets that consisted of 32 constants (16 reaction rate constants and 16 Michaelis-Menten constants) and then numerically solved the equations to find chaotic parameter sets. Reaction rate constants k_{a1} - k_{a8} and k_{b1} - k_{b8} were independently generated from exponential distributions bounded between 1 and 1000 min^{-1} . Michaelis-Menten constants K_{ma1} - K_{ma8} and K_{mb1} - K_{mb8} were independently generated from exponential distributions bounded between

0.01 and 1000 μM . The integration began from a state in which all the substrate molecules were dephosphorylated and all the enzyme molecules were unbound ($[\text{S}_{a00}] = [\text{S}_{b00}] = 1000 \mu\text{M}$; $[\text{E}] = [\text{F}] = 20 \mu\text{M}$). The solution for each parameter set could be convergent, oscillatory, or chaotic. We judged a solution to be chaotic when its power spectrum was continuous rather than discrete; the spectrum was firstly numerically classified as not discrete if the proportion of the power at the peak frequency to the total power was below 15%. Then we plotted those candidate continuous spectrums and visually checked their continuity. We further checked the chaotic parameter sets to ensure that, after sufficient time had passed ($t = 5000 \text{ min}$), the solution was divergent because of small changes in the initial state of the integration. The degree of divergence is visually inspected. Oscillatory parameter sets were collected in the same manner as chaotic parameter sets. Solutions were considered to be oscillatory when the power spectrum was discrete.

Clustering of chaotic parameter sets

Chaotic parameter sets collected in the random parameter search were standardized and clustered by performing a clustering analysis. In the standardization procedure, each constant was transformed so that the defined lower bound, upper bound, and the midpoint between them mapped to -1 , 1 , and 0 , respectively. To achieve this, reaction rate constants were log-transformed with base 10, 1.5 was subtracted from the value $[\text{=} (0 + 3)/2]$, and then this value was divided by $1.5 [\text{=} (3 - 0)/2]$. Michaelis–Menten constants were log-transformed with base 10, 0.5 was subtracted from the value $[\text{=} (3 + (-2))/2]$, and then this value was divided by $2.5 [\text{=} (3 - (-2))/2]$. In the clustering analysis, standardized parameters were hierarchically clustered using Ward's algorithm. We used a special distance metric for the algorithm to consider the three symmetries of the system. These symmetries existed (1) in the phosphorylation states of each substrate (i.e., exchanging the position of S_{a01} and S_{a10} , or exchanging the position of S_{b01} and S_{b10} , conserves the overall structure), (2) as an enzymatic symmetry (i.e., exchanging the role of kinase and phosphatase conserves the overall structure), and (3) as a substrate symmetry (i.e., exchanging S_a and S_b conserves the overall structure). By considering the first symmetry, the parameter set that exchanged parameter $\{k_{a1}, K_{ma1}, k_{a2}, K_{ma2}, k_{a3}, K_{ma3}, k_{a4}, K_{ma4}, k_{a5}, K_{ma5}, k_{a6}, K_{ma6}, k_{a7}, K_{ma7}, k_{a8}, K_{ma8}\}$ with $\{k_{a2}, K_{ma2}, k_{a1}, K_{ma1}, k_{a4}, K_{ma4}, k_{a3}, K_{ma3}, k_{a6}, K_{ma6}, k_{a5}, K_{ma5}, k_{a8}, K_{ma8}, k_{a7}, K_{ma7}\}$ can be regarded as the same as the original set. Similarly, by considering the second symmetry, the parameter set that exchanged parameter $\{k_{a1}, K_{ma1}, k_{a2}, K_{ma2}, k_{a3}, K_{ma3}, k_{a4}, K_{ma4}, k_{a5}, K_{ma5}, k_{a6}, K_{ma6}, k_{a7}, K_{ma7}, k_{a8}, K_{ma8}, k_{b1}, K_{mb1}, k_{b2}, K_{mb2}, k_{b3}, K_{mb3}, k_{b4}, K_{mb4}, k_{b5}, K_{mb5}, k_{b6}, K_{mb6}, k_{b7}, K_{mb7}, k_{b8}, K_{mb8}\}$ with $\{k_{b7}, K_{mb7}, k_{b8}, K_{mb8}, k_{b5}, K_{mb5}, k_{b6}, K_{mb6}, k_{b3}, K_{mb3}, k_{b4}, K_{mb4}, k_{b1}, K_{mb1}, k_{b2}, K_{mb2}, k_{b7}, K_{mb7}, k_{b8}, K_{mb8}, k_{b5}, K_{mb5}, k_{b6}, K_{mb6}, k_{b3}, K_{mb3}, k_{b4}, K_{mb4}, k_{b1}, K_{mb1}, k_{b2}, K_{mb2}\}$ can be regarded as the same set. By considering the third symmetry, the parameter set that exchanged parameter $\{k_{a1}, K_{ma1}, k_{a2}, K_{ma2}, k_{a3}, K_{ma3}, k_{a4}, K_{ma4}, k_{a5}, K_{ma5}, k_{a6}, K_{ma6}, k_{a7}, K_{ma7}, k_{a8}, K_{ma8}, k_{b1}, K_{mb1}, k_{b2}, K_{mb2}, k_{b3}, K_{mb3}, k_{b4}, K_{mb4}, k_{b5}, K_{mb5}, k_{b6}, K_{mb6}, k_{b7}, K_{mb7}, k_{b8}, K_{mb8}\}$ with $\{k_{b1}, K_{mb1}, k_{b2}, K_{mb2}, k_{b3}, K_{mb3}, k_{b4}, K_{mb4}, k_{b5}, K_{mb5}, k_{b6}, K_{mb6}, k_{b7}, K_{mb7}, k_{b8}, K_{mb8}, k_{a1}, K_{ma1}, k_{a2}, K_{ma2}, k_{a3}, K_{ma3}, k_{a4}, K_{ma4}, k_{a5}, K_{ma5}, k_{a6}, K_{ma6}, k_{a7}, K_{ma7}, k_{a8}, K_{ma8}\}$ can be regarded as the same set. Given

these symmetries, the distance between two parameter sets P_1 and P_2 is defined as the minimum of the distances between P_1 and all the symmetrically exchangeable parameter sets of P_2 . To abstract the motif structure, parameter histograms were calculated for each cluster. When observing the distribution of all parameters in all clusters (**Figures 2 and S2**), the highest frequency at which parameters occurred with highly skewed distributions was ~ 0.4 . Therefore, we set a threshold value of 0.2, i.e., half the highest frequency.

Biased parameter search

Parameter sets were generated by introducing some specific biases to some of their parameters; the solutions were then classified in the same manner as for the random parameter search based on the power spectrum. The biases were determined as combinations of motif A bias and motif B bias. Both motif A bias and motif B bias consisted of two biased parameters, one for a high reaction rate constant and the other for a low Michaelis–Menten constant. When the bias for the reaction rate constant was set, the parameter was randomly generated from an exponential distribution bounded between 100 and 1000 min^{-1} . When the bias for the Michaelis–Menten constant was set, the parameter was randomly generated from an exponential distribution bounded between 0.01 and 0.1 μM . In this biased parameter search, we did not apply visual inspection of the sensitivity to initial conditions. The lack of this confirmation would not critically deteriorate the classification performance for a chaos parameter set: for a follow-up analysis, we randomly chose 1,000 parameter sets that were classified as chaos through all the biased conditions and inspected their sensitivity to initial conditions. Through the inspection, only 12 parameters were found to be misclassified (in other words, 98.8% of chaos parameters were accurately classified as chaos without the visual inspection of initial condition sensitivity).

Collection of stereotypical chaos and oscillatory parameter sets

To obtain stereotypical chaos parameter sets with symmetrical structures, we used the results of the biased parameter search corresponding to motif arrangement #46. Parameters were randomly sampled from a Gaussian distribution defined by the mean and the covariance matrix of chaos parameters obtained from the biased parameter search. In this sampling, distributions were not bounded within a specific range. The sampled parameter was modified so that it had a symmetrical structure, i.e., $k_{ai} = k_{a(9-i)}$, $k_{bi} = k_{b(9-i)}$, $K_{mai} = K_{ma(9-i)}$, $K_{mbi} = K_{mb(9-i)}$ for $i = 1 \dots 4$. The solution was then determined to be either chaotic or not chaotic as described in the method section “Random parameter search for chaotic and oscillatory parameter sets”. In total, 97 chaotic parameters were collected from 10 million random sampling repeats. Chaotic parameters were confirmed to show initial condition sensitivity. The stereotypical oscillatory parameter sets were obtained by the same procedure except that the numerical solution was considered to be oscillation. Collection of oscillatory parameter sets continued until 97 sets were found.

The example chaos parameter set was selected as follows. Each stereotypical chaos

parameter set was first standardized, which was conducted using the same method described for the clustering procedure. The example parameter set was then selected as the one closest to the mean of the standardized parameter sets. The distance between parameter sets was measured by Euclidian distance. The values of the selected stereotypical chaos parameter sets are shown in **Table S1**.

Bifurcation analysis

Each parameter in the typical chaotic parameter set varied between the following ranges: 1 and 1000 min⁻¹ for the reaction rate constant; 0.01 and 0.1 μM for the binding constant. The varied value took 30 logarithmically-spaced points between the ranges, including both sides. For each analysis, the solution type was determined as described in the method section “Random parameter search for chaotic and oscillatory parameter sets”. For asymmetric perturbation, when bifurcation analysis on each specific parameter had been conducted, the other parameters at the symmetrical positions were fixed to the original value, resulting in a violation of symmetry. For symmetric perturbation, both parameters at the symmetrical positions (e.g., k_{a1} and k_{a8}) varied simultaneously. Bifurcation maps were produced based on the results of the bifurcation analysis. The color of each cell was specified using a RGB color code: the R channel was set to the proportion of chaos behavior, G was the proportion of oscillation, and B was the proportion of convergence.

Stochastic simulation

The stochastic simulation was performed using Gillespie’s direct method stochastic simulation algorithm implemented in StochPy (Maarleveld et al., 2013). We modified the simulation to track the behavior of the full system including each kinase–substrate complex molecule. The full ordinary differential equation system, without application of the Michaelis–Menten approximation, is described below.

$$\frac{d[S_{a00}]}{dt} = -(k_{ca1} + k_{ca2})[E][S_{a00}] + k_{uca1}[ES_{a00 \rightarrow a01}] + k_{uca2}[ES_{a00 \rightarrow a10}] + k_{a5}[FS_{a01}] + k_{a6}[FS_{a10}] \quad (11)$$

$$\frac{d[S_{a01}]}{dt} = -k_{ca3}[E][S_{a01}] + k_{uca3}[ES_{a01}] - k_{ca5}[F][S_{a01}] + k_{uca5}[FS_{a01}] + k_{a1}[ES_{a00 \rightarrow a01}] + k_{a7}[FS_{a11 \rightarrow a01}] \quad (12)$$

$$\frac{d[S_{a10}]}{dt} = -k_{ca4}[E][S_{a10}] + k_{uca4}[ES_{a10}] - k_{ca6}[F][S_{a10}] + k_{uca6}[FS_{a10}] + k_{a2}[ES_{a00 \rightarrow a10}] + k_{a8}[FS_{a11 \rightarrow a10}] \quad (13)$$

$$\frac{d[S_{a11}]}{dt} = -(k_{ca7} + k_{ca8})[F][S_{a11}] + k_{uca7}[FS_{a11 \rightarrow a01}] + k_{uca8}[FS_{a11 \rightarrow a10}] + k_{a3}[ES_{a01}] + k_{a4}[ES_{a10}] \quad (14)$$

$$\frac{d[ES_{a00 \rightarrow a01}]}{dt} = k_{ca1}[E][S_{a00}] - (k_{uca1} + k_{a1})[ES_{a00 \rightarrow a01}] \quad (15)$$

$$\frac{d[ES_{a00 \rightarrow a10}]}{dt} = k_{ca2}[E][S_{a00}] - (k_{uca2} + k_{a2})[ES_{a00 \rightarrow a10}] \quad (16)$$

$$\frac{d[ES_{a01}]}{dt} = k_{ca3}[E][S_{a01}] - (k_{uca3} + k_{a3})[ES_{a01}] \quad (17)$$

$$\frac{d[ES_{a10}]}{dt} = k_{ca4}[E][S_{a10}] - (k_{uca4} + k_{a4})[ES_{a10}] \quad (18)$$

$$\frac{d[FS_{a01}]}{dt} = k_{ca5}[F][S_{a01}] - (k_{uca5} + k_{a5})[FS_{a01}] \quad (19)$$

$$\frac{d[FS_{a10}]}{dt} = k_{ca6}[F][S_{a10}] - (k_{uca6} + k_{a6})[FS_{a10}] \quad (20)$$

$$\frac{d[FS_{a11 \rightarrow a01}]}{dt} = k_{ca7}[F][S_{a11}] - (k_{uca7} + k_{a7})[FS_{a11 \rightarrow a01}] \quad (21)$$

$$\frac{d[FS_{a11 \rightarrow a10}]}{dt} = k_{ca8}[F][S_{a11}] - (k_{uca8} + k_{a8})[FS_{a11 \rightarrow a10}] \quad (22)$$

$$\begin{aligned} \frac{d[S_{b00}]}{dt} = & -(k_{cb1} + k_{cb2})[E][S_{b00}] + k_{ucb1}[ES_{b00 \rightarrow b01}] \\ & + k_{ucb2}[ES_{b00 \rightarrow b10}] + k_{b5}[FS_{b01}] + k_{b6}[FS_{b10}] \end{aligned} \quad (23)$$

$$\begin{aligned} \frac{d[S_{b01}]}{dt} = & -k_{cb3}[E][S_{b01}] + k_{ucb3}[ES_{b01}] - k_{cb5}[F][S_{b01}] \\ & + k_{ucb5}[FS_{b01}] + k_{b1}[ES_{b00 \rightarrow b01}] + k_{b7}[FS_{b11 \rightarrow b01}] \end{aligned} \quad (24)$$

$$\begin{aligned} \frac{d[S_{b10}]}{dt} = & -k_{cb4}[E][S_{b10}] + k_{ucb4}[ES_{b10}] - k_{cb6}[F][S_{b10}] \\ & + k_{ucb6}[FS_{b10}] + k_{b2}[ES_{b00 \rightarrow b10}] + k_{b8}[FS_{b11 \rightarrow b10}] \end{aligned} \quad (25)$$

$$\begin{aligned} \frac{d[S_{b11}]}{dt} = & -(k_{cb7} + k_{cb8})[F][S_{b11}] + k_{ucb7}[FS_{b11 \rightarrow b01}] \\ & + k_{ucb8}[FS_{b11 \rightarrow b10}] + k_{b3}[ES_{b01}] + k_{b4}[ES_{b10}] \end{aligned} \quad (26)$$

$$\frac{d[ES_{b00 \rightarrow b01}]}{dt} = k_{cb1}[E][S_{b00}] - (k_{ucb1} + k_{b1})[ES_{b00 \rightarrow b01}] \quad (28)$$

$$\frac{d[ES_{b00 \rightarrow b10}]}{dt} = k_{cb2}[E][S_{b00}] - (k_{ucb2} + k_{b2})[ES_{b00 \rightarrow b10}] \quad (29)$$

$$\frac{d[ES_{b01}]}{dt} = k_{cb3}[E][S_{b01}] - (k_{ucb3} + k_{b3})[ES_{b01}] \quad (30)$$

$$\frac{d[ES_{b10}]}{dt} = k_{cb4}[E][S_{b10}] - (k_{ucb4} + k_{b4})[ES_{b10}] \quad (31)$$

$$\frac{d[FS_{b01}]}{dt} = k_{cb5}[F][S_{b01}] - (k_{ucb5} + k_{b5})[FS_{b01}] \quad (32)$$

$$\frac{d[FS_{b10}]}{dt} = k_{cb6}[F][S_{b10}] - (k_{ucb6} + k_{b6})[FS_{b10}] \quad (33)$$

$$\frac{d[FS_{b11 \rightarrow b01}]}{dt} = k_{cb7}[F][S_{b11}] - (k_{ucb7} + k_{b7})[FS_{b11 \rightarrow b01}] \quad (34)$$

$$\frac{d[FS_{b11 \rightarrow b10}]}{dt} = k_{cb8}[F][S_{b11}] - (k_{ucb8} + k_{b8})[FS_{b11 \rightarrow b10}] \quad (35)$$

$$\begin{aligned} \frac{d[E]}{dt} = & -((k_{ca1} + k_{ca2})[S_{a00}] + k_{ca3}[S_{a01}] + k_{ca4}[S_{a10}])[E] + (k_{uca1} + k_{a1})[ES_{a00 \rightarrow a10}] \\ & + (k_{uca2} + k_{a2})[ES_{a00 \rightarrow a10}] + (k_{uca3} + k_{a3})[ES_{a01}] + (k_{uca4} + k_{a4})[ES_{a10}] \\ & - ((k_{cb1} + k_{cb2})[S_{b00}] + k_{cb3}[S_{b01}] + k_{cb4}[S_{b10}])[E] + (k_{ucb1} + k_{b1})[ES_{b00 \rightarrow b01}] \\ & + (k_{ucb2} + k_{b2})[ES_{b00 \rightarrow b10}] + (k_{ucb3} + k_{b3})[ES_{b01}] + (k_{ucb4} + k_{b4})[ES_{b10}] \end{aligned} \quad (36)$$

$$\begin{aligned} \frac{d[F]}{dt} = & -(k_{ca5}[S_{a00}] + k_{ca6}[S_{a10}] + (k_{ca7} + k_{ca8})[S_{a11}])[F] + (k_{uca5} + k_{a5})[FS_{01}] \\ & + (k_{uca6} + k_{a6})[FS_{a10}] + (k_{uca7} + k_{a7})[FS_{a11 \rightarrow a01}] + (k_{uca8} + k_{a8})[FS_{a11 \rightarrow a10}] \\ & - (k_{cb5}[S_{b00}] + k_{cb6}[S_{b10}] + (k_{cb7} + k_{cb8})[S_{b11}])[F] + (k_{ucb5} + k_{b5})[FS_{01}] \\ & + (k_{ucb6} + k_{b6})[FS_{b10}] + (k_{ucb7} + k_{b7})[FS_{b11 \rightarrow b01}] + (k_{ucb8} + k_{b8})[FS_{b11 \rightarrow b10}] \end{aligned} \quad (37)$$

In these equations, $[S_{a00}]$, $[S_{a01}]$, $[S_{a10}]$, and $[S_{a11}]$ represent the concentrations of the four phosphorylation states of substrate A; $[S_{b00}]$, $[S_{b01}]$, $[S_{b10}]$, and $[S_{b11}]$ represent the concentrations of the four phosphorylation states of substrate B; $[E]$ and $[F]$ are the concentrations of free (unbound) kinase and phosphatase; $[ES]$ and $[FS]$ are the enzyme-substrate complex concentrations with the arrow in the subscript indicating which reaction the complex is involved in (e.g., $ES_{a00 \rightarrow a01}$ denotes that the ES complex is involved in the kinase reaction converting S_{a00} to S_{a01}); k_{a1} - k_{a8} and k_{b1} - k_{b8} are the catalytic rate constants; k_{ca1} - k_{ca8} and k_{cb1} - k_{cb8} are the binding constants; and k_{uca1} - k_{uca8} and k_{ucb1} - k_{ucb8} are the unbinding constants. The values of the parameter sets are shown in **Table S2**. The relationship among the Michaelis-Menten constants, binding constants, and unbinding constants is described as follows:

$$K_{mi} = \frac{k_{uci} + k_i}{k_{ci}}, \text{ for } i = 1 \dots 8 \quad (38)$$

Software for computer simulation

Numerical integration and clustering were carried out by Python 3.6.1 with the libraries of numpy 1.12.1 and scipy 0.19.1, or by Mathematica 12.0 (Wolfram Research). Stochastic simulation was carried out by StochPy 2.3.